Thomson scattering of intense lasers from electron beams at arbitrary interaction angles

Sally K. Ride,[1] Eric Esarey,[2] and Michael Baine[1]
[1]*Department of Physics and California Space Institute, University of California, San Diego, La Jolla, California 92093-0221*
[2]*Beam Physics Branch, Plasma Physics Division, Naval Research Laboratory, Washington, D.C. 20375-5346*
(Received 18 May 1995)

Analysis of nonlinear Thomson scattering of intense lasers from relativistic electron beams is extended to describe off-axis scattering geometries. Electron trajectories are calculated for the case of a plane electromagnetic wave of arbitrary intensity, either circularly or linearly polarized, interacting with a relativistic electron beam at an arbitrary interaction angle. The trajectories are used to derive analytic expressions for the intensity distribution of the scattered radiation. These expressions are valid in the nonlinear regime (arbitrary laser intensity) and include the generation of harmonics. The effect of interaction angle on the intensity distribution is discussed and spectra are plotted numerically for the specific cases of head-on and transverse scattering. The dependence of x-ray frequency, pulse duration, and photon flux on interaction geometry are also examined. Applications to the laser synchrotron source are discussed. There are potential advantages of both head-on and transverse interaction geometries: head-on scattering results in the generation of higher frequencies and higher photon fluxes; normal incidence scattering can result in ultrashort x-ray pulses.

PACS number(s): 41.75.Ht, 41.60.Ap, 41.75.Fr, 52.40.Nk

I. INTRODUCTION

Recently there has been considerable interest in the possibility of designing a compact source of x rays based on the Thomson scattering of intense laser fields from electron beams [1–10]. An x-ray source based on this mechanism, referred to as a laser synchrotron source (LSS) [5–7], could produce short pulses of tunable, narrow band x rays, and thus have many applications in medicine, biological science, and materials science. Such a source is now practical, due in part to advances in solid-state laser technology, which have made compact sources of ultraintense laser radiation available [11–13].

In a previous paper, we developed a detailed theory to describe the nonlinear Thomson scattering of intense laser fields from beams and plasmas [1]. This theory described scattering of linearly or circularly polarized laser fields of arbitrary intensities, but was limited to a colinear geometry (that is, when the laser pulse and electron beam meet head-on). In the present paper, we generalize our previous results to describe nonlinear Thomson scattering, and the radiation that results, when the laser pulse and the electrons meet at an arbitrary angle. Expressions for the intensity distributions are obtained for both linearly and circularly polarized incident laser fields of arbitrary intensities. This work is based on classical radiation theory, which is valid as long as the energy of the radiated photon is much less than the electron energy, $\hbar\omega \ll \gamma mc^2$; for an incident laser of the type now available, with wavelength ~ 1 μm (intensity $\geq 10^{18}$ W/cm^2 and laser strength parameter $a_0 \sim 1$), this implies electron energies below ~ 50 GeV.

Extending the analytic description of nonlinear Thomson scattering to off-axis angles is important for several reasons. First, there may be practical constraints on realistic experimental configurations that preclude the use of head-on interaction geometry; this work allows calculation of the radiation pattern for a particular experimental setup. Second, there are specific advantages to different scattering geometries; for example, since the x-ray pulse length is determined by the interaction time, transverse scattering provides a means to achieve ultrashort (< 1 ps) x-ray pulses [9]. There may also be advantages to being able to change the interaction geometry; as an example, changing the interaction angle is one way of tuning the x-ray frequency. Further, the analytic expressions obtained in this paper provide the tools to calculate the spatial and spectral distribution of radiation from real electron beams interacting with real laser pulses. Since the expressions derived are functions of electron energy and incident angle, they enable analysis of beams with finite emittance and energy spread.

The idea of producing high energy photons by scattering laser light off relativistic electron beams is not new. Thomson scattering (or inverse Compton scattering) in the linear regime was discussed by Arutyumian and Tumanian [14], and Milburn [15] in the early 1960s, and has since been explored in several experiments (both as an electron beam diagnostic [16,17], and as a method of producing x rays and γ rays [18–22]). Nonlinear Thomson scattering from a single electron initially at rest was first examined analytically in the classic work of Sarachik and Schappert [2]. Our previous work extended and generalized those results [1], and examined in detail the properties of the radiation that results from nonlinear Thomson scattering (again, in a head-on geometry). Several authors [23–32] have analyzed the synchrotron radiation produced as relativistic electrons travel through a static, periodic transverse magnetic field. This process is quite similar to Thomson scattering, as can be seen by viewing the interaction in the electron frame, a frame in which the static, transverse field appears as (very nearly) a radi-

ation field. All work on the details of the radiation patterns has been confined to head-on interaction geometry.

A laser synchrotron source is somewhat analogous to a conventional synchrotron source. In a conventional source, x rays are generated by a high energy electron beam passing through the periodic, transverse magnetic field of an undulator (or wiggler) magnet. X rays are generated along the electron beam axis with a wavelength $\lambda=\lambda_u/2\gamma^2$, where λ_u is the undulator wavelength and γ is the relativistic factor of the electron beam. Similarly, in the LSS, x rays are generated as an electron beam passes through the laser radiation field. For head-on geometry, backscattered x rays are generated along the electron beam axis at a wavelength $\lambda=\lambda_0/4\gamma^2$, where λ_0 is the laser wavelength. (The above assume the dimensionless field strengths of the undulator field and the laser field are $\ll 1$.) Since the typical laser wavelength ($\lambda_0\approx 1$ μm) is some four orders of magnitude shorter than the typical undulator wavelength ($\lambda_u\approx 4$ cm), an LSS requires a much lower energy electron beam to produce a given wavelength x ray. For example, in order to generate 30 keV ($\lambda=4$ nm) x rays, a conventional synchrotron source with $\lambda_u=4$ cm requires a very high electron beam, $E_b=12$ GeV; in contrast, an LSS employing a laser of wavelength $\lambda_0=1$ μm requires only $E_b=40$ MeV, an energy that is typical of those available from compact rf linacs, and a factor of 300 less than that required by the conventional synchrotron source. Because a much lower electron beam energy is needed to produce a particular photon energy, the LSS can employ more compact electron accelerators, and thus can be relatively compact itself, particularly when compared to conventional synchrotron sources.

The laser synchrotron source has several other attractive features: the x rays are near-monochromatic (bandwidth typically a few percent), are well collimated (in a cone of $\theta_c\sim 1/\gamma$ in the direction of the electron beam), and are tunable over a broad portion of the x-ray spectrum (by varying electron energy or interaction angle). Further, the x rays can be emitted in extremely short pulses, and the polarization can be changed by changing the polarization of the incident laser.

The dimensionless laser strength parameter a_0 plays an important role in determining the character of the emitted radiation. a_0 is the normalized amplitude of the vector potential of the incident laser field, $a_0=eA_0/m_ec^2$ (just as K, the undulator strength parameter, is the normalized amplitude of the vector potential of the undulator magnetic field), and is related to the intensity I_0 of the laser by

$$a_0\approx 0.85\times 10^{-9}[\lambda_0\ (\mu\text{m})][I_0\ (\text{W/cm}^2)]^{1/2}\ . \qquad (1)$$

When $a_0\ll 1$, scattering occurs in the linear regime. Radiation is generated at the (Doppler upshifted) fundamental frequency. When $a_0\geq 1$, scattering occurs in the nonlinear regime, and radiation is generated in the fundamental and in higher harmonics. State-of-the-art compact laser systems based on chirped-pulse amplification [11–13] can currently deliver ultrashort pulses (<1 ps) at ultrahigh power (>10 TW) and intensity ($>10^{18}$ W/cm^2, corresponding to $a_0\sim 1$ for a laser of wavelength 1 μm). Thus, lasers which can be used to explore Thomson scattering in the nonlinear regime exist.

For off-axis geometries, in the nonlinear regime, the frequency of backscattered radiation (radiation emitted in the direction of the electron's average motion in the laser field) is given approximately by $\omega=\omega_0 2\gamma^2 n(1+\beta_{z0})/(1+a_0^2/2)$, where ω_0 is the laser frequency, n is the harmonic number, and β_{z0} is that component of the electron's initial velocity which is directed toward the oncoming laser pulse (which travels in the $-z$ direction). For head-on interactions, $\beta_{z0}\sim 1$; for off-axis interactions, β_{z0} decreases as the scattering angle increases. There are several things to notice about this relation. First, the radiated frequency is increased by a relativistic Doppler factor, which varies from $\sim 4\gamma^2$ for head-on scattering to $\sim 2\gamma^2$ for transverse scattering. (This dependence of radiated frequency on initial scattering angle is familiar from inverse Compton scattering in the low a_0 limit, and is easily understood by viewing the process in the average electron frame: the electron sees a laser pulse of Doppler shifted frequency that depends on scattering angle; it then emits radiation in the forward direction, which undergoes a second Doppler shift when transformed to the observer's frame.) Second, the intensity of the laser induces a frequency shift; the frequency of backscattered radiation is reduced by a factor of $(1+a_0^2/2)$. Finally, the frequency of harmonics increases with harmonic number. Harmonics become important in the nonlinear regime, when $a_0\approx 1$. For ultrahigh intensities, $a_0^2\gg 1$, numerous harmonics are generated, and the result is a near continuum of scattered radiation with harmonics extending out to some critical harmonic number, $n_c\sim a_0^3$, beyond which the intensity of the scattered radiation rapidly decreases [1]. [Note that this also implies that an ultraintense laser incident on a stationary plasma ($\gamma_0=1$) can be used to produce soft x rays by generating radiation in high harmonics, i.e., $\lambda=\lambda_0/n$ [1].] The generation of significant radiation into high harmonics (possible with current state-of-the-art lasers) provides an additional avenue to pursue in order to obtain high frequency radiation.

With high laser intensities ($a_0\sim 1$), it is possible to generate high peak fluxes of x rays. A laser synchrotron source could be designed to produce high peak fluxes of ultrashort pulse (≤ 1 ps) x rays using a high intensity, short pulse, chirped-pulse-amplification laser system in conjunction with a high peak current rf linac. The average flux of such a configuration will be limited by the average power (repetition rate) of the laser and/or electron beam. It is also possible to design an LSS to operate at high average flux. This requires the use of a high average power laser (such as a diode-pumped solid-state system) and a high average current electron accelerator (such as a betatron or a high repetition rate linac). The possibility of using "super" cavities to store and confine an input laser beam [10] or the use of a ring resonator laser configuration [7] have been suggested as methods for generating high average flux, and the backscattering of radiation in a high power free electron laser is also being explored [4]. The choice of whether to design an LSS

for high peak or high average flux would depend on the particular x-ray application; both are now feasible.

In this paper we extend our previous results, which considered only head-on laser-electron interaction, to describe off-axis scattering geometries as well. In Sec. II, we calculate the electron orbits for the case of a plane electromagnetic wave, either circularly or linearly polarized, interacting with an electron beam of arbitrary energy at arbitrary interaction angles. The coordinate systems and transformations are defined in Sec. III. Then, in Sec. IV, the electron orbits in the laser field are used to derive analytic expressions for the intensity distribution of the scattered radiation. The expressions obtained are valid in the nonlinear regime (arbitrary laser intensity) and include the generation of harmonics. In Sec. V, the effect of interaction angle on the intensity distribution is discussed, and spectra are plotted numerically for the specific cases of $\theta_I=0°$, 90°, where θ_I is the laser-electron beam interaction angle. These plots show the intensity of radiation into the first three harmonics for both linear and circular polarization, and illustrate the effect of off-axis geometries on the radiation pattern. In Sec. VI, we discuss the effects of interaction angle on the x-ray pulse duration and the photon flux. This paper does not consider various nonideal effects, such as finite electron energy spread, electron beam emittance, and nonuniformities in the laser pulse intensity; this will be the subject of future work.

II. ELECTRON MOTION IN INTENSE LASER FIELDS

The equations of motion of an electron interacting with a laser pulse are determined by the radiation field of the laser and the space-charge field of the electron beam. Under certain conditions, the effect of the space-charge field can be neglected. In this section, we derive the general equations describing electron motion in the combined fields, then show that for electron beams of interest in this application only the laser field need be considered.

The laser field and space-charge field can be represented using the normalized vector and scalar potentials, $\mathbf{a}=e\mathbf{A}/m_ec^2$ and $\hat{\Phi}=e\Phi/m_ec^2$, respectively, where m_e is the electron mass, e is the magnitude of the electron charge, and c is the speed of light. In the Coulomb gauge, $\nabla\cdot\mathbf{a}=0$ implies $a_z=0$ in one dimension (1D). Then, $a_\perp$ represents the laser field and $\hat{\Phi}$ represents the space-charge field.

The normalized vector potential of a laser radiation field of arbitrary polarization is represented by

$$\mathbf{a}=(a_0/\sqrt{2})[(1+\delta_p)^{1/2}\cos(k_0\eta)\mathbf{e}_x + (1-\delta_p)^{1/2}\sin(k_0\eta)\mathbf{e}_y] , \quad (2)$$

where $\delta_p=1$ for linear polarization and $\delta_p=0$ for circular polarization, $k_0=2\pi/\lambda_0$ is the wave number of the laser field, and $\eta=z+ct$ (describing light traveling in the $-z$ direction). Using this representation, $(a^2)_s=a_0^2/2$ for both linear and circular polarizations, where the subscript s signifies the slow component (an averaging over the laser wavelength). In the following, the laser field is assumed to be moving to the left ($-z$ direction) and the electrons are initially (prior to the interaction with the laser field) moving with velocity $\mathbf{v}_0=v_{x0}\mathbf{e}_x+v_{y0}\mathbf{e}_y+v_{z0}\mathbf{e}_z$ (see Fig. 1).

The electron motion in the fields $\mathbf{a}$ and $\hat{\Phi}$ is governed by the relativistic Lorentz equation, which may be written in the form

$$\frac{1}{c}\frac{d}{dt}\mathbf{u}=\nabla\hat{\Phi}+\frac{1}{c}\frac{\partial}{\partial t}\mathbf{a}-\boldsymbol{\beta}\times(\nabla\times\mathbf{a}) , \quad (3)$$

where $\boldsymbol{\beta}=\mathbf{v}/c$ is the normalized electron velocity, $\mathbf{u}=\mathbf{p}/m_ec=\gamma\boldsymbol{\beta}$ is the normalized electron momentum, and $\gamma=(1+u^2)^{1/2}=(1-\beta^2)^{-1/2}$ is the relativistic factor. Assuming that the laser field, $\mathbf{a}_\perp$, and hence the quantities $\hat{\Phi}$, $\boldsymbol{\beta}$, $\mathbf{u}$, and γ are functions only of the variable $\eta=z+ct$, Eq. (3) implies the existence of two constants of the motion [1,33,34],

$$\frac{d}{d\eta}(\mathbf{u}_\perp-\mathbf{a}_\perp)=\mathbf{0} , \quad (4a)$$

$$\frac{d}{d\eta}(\gamma+u_z-\hat{\Phi})=0 . \quad (4b)$$

Equation (4a) is just conservation of canonical transverse momentum in 1D, and Eq. (4b) can be interpreted as conservation of energy in the wave frame. Equations (4a) and (4b) can be integrated to give

$$\mathbf{u}_\perp=\mathbf{a}_\perp+\mathbf{u}_{\perp 0} , \quad (5a)$$

$$\gamma+u_z-\hat{\Phi}=\gamma_0+u_{z0} , \quad (5b)$$

where, prior to the laser interaction (when $\mathbf{a}_\perp=\mathbf{0}$), $\mathbf{u}_\perp=\mathbf{u}_{\perp 0}$, $\hat{\Phi}=0$, $u_z=u_{z0}$, and $\gamma=\gamma_0=(1+u_{z0}^2+u_{\perp 0}^2)^{1/2}$. The two constants of the motion, Eqs. (5a) and (5b), completely describe the nonlinear motion of electrons in the potentials $\mathbf{a}$ and $\hat{\Phi}$. They allow the electron motion to be

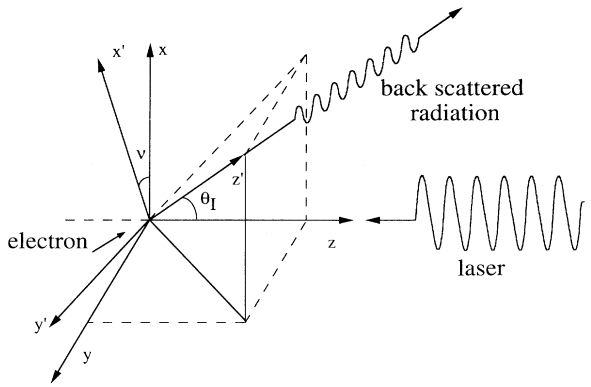

FIG. 1. Schematic diagram showing Thomson scattering of an intense laser field by a free electron, and the relationship between the two Cartesian coordinate systems used in this paper. The laser pulse travels in the -z direction, so the (x,y,z) system is used to calculate electron trajectories; the electron's average motion (during its interaction with the laser) is in the z' direction, and therefore the spherical coordinates used in the radiation calculation are defined in reference to the (x',y',z') system. The angles θ_I and ν are the angles between the z and z' and x and x' axes, respectively.

specified solely in terms of the fields, i.e.,

$$\beta_z=\frac{h_0^2-(1+u_\perp^2)}{h_0^2+(1+u_\perp^2)}\ , \tag{6a}$$

$$\gamma=(h_0^2+1+u_\perp^2)/2h_0\ , \tag{6b}$$

$$\boldsymbol{\beta}_\perp=(\mathbf{a}_\perp+\mathbf{u}_{\perp 0})/\gamma\ , \tag{6c}$$

where $h_0=\gamma_0+u_{z0}+\hat{\Phi}$.

For typical electron beams of interest, it can be shown that the electrostatic potential is sufficiently small that it can be neglected, and consequently $h_0\approx\gamma_0+u_{z0}$. In general, $\hat{\Phi}=\hat{\Phi}^{(0)}+\hat{\Phi}^{(1)}$, where $\hat{\Phi}^{(0)}$ is the initial equilibrium space-charge potential (prior to interaction with the laser pulse) and $\hat{\Phi}^{(1)}$ is the potential due to the presence of the laser field. For a long, axially uniform electron beam, $|\hat{\Phi}^{(0)}|\le\nu_b$, where $\nu_b=[I_b\ (\mathrm{kA})]/17\beta_0$ is the Budker parameter and I_b (kA) is the beam current. Since $\nu_b\ll 1$ for beams of interest, $\hat{\Phi}^{(0)}$ can be neglected. The space-charge potential induced by the laser pulse, $\hat{\Phi}^{(1)}$, can be neglected provided that the laser-electron interaction time T_0 is short compared to an effective electron plasma period, i.e., $T_0\ll\omega_p^{-1}\gamma_0^{3/2}(1+\beta_{z0})/(1+a_0^2/8)^{1/2}$, where $\omega_p=(4\pi e^2 n_e/m_e)^{1/2}$ is the plasma frequency and n_e is the ambient electron density. Taking $\beta_{z0}\sim 1$ and $a_0^2\ll 8$, this can be written as $T_0\ (\mu\mathrm{s})\ll 35\gamma_0^{3/2}[n_e\ (\mathrm{cm}^{-3})]^{-1/2}$. For example, $T_0\ll 3.5\gamma_0^{3/2}$ ps for $n_e=10^{14}\ \mathrm{cm}^{-3}$. In this "short-pulse" limit, $\hat{\Phi}^{(1)}$ can be neglected, the constant of motion in Eq. (5b) becomes $\gamma+u_z=\gamma(1+\beta_z)$, and h_0 is given by

$$h_0=\gamma_0(1+\beta_{z0})\ . \tag{7}$$

The quantity $\hat{\Phi}^{(1)}$ can also be estimated in the opposite limit, appropriate for laser interaction with plasmas [1]. The remainder of this paper will be concerned with laser-electron interactions in the short-pulse regime.

The electron orbits, $\mathbf{r}(\eta)=x(\eta)\mathbf{e}_x+y(\eta)\mathbf{e}_y+z(\eta)\mathbf{e}_z$, can be calculated as a function of η using Eqs. (6a)–(6c) and the relation

$$\frac{1}{c}\frac{d\mathbf{r}}{dt}=\boldsymbol{\beta}=(1+\beta_z)\frac{d\mathbf{r}}{d\eta}\ , \tag{8}$$

which gives $d\mathbf{r}/d\eta=\mathbf{u}/h_0$. Using the general form for the laser field given by Eq. (2), the normalized components of the electron momentum are given by

$$u_x=\frac{a_0}{\sqrt{2}}(1+\delta_p)^{1/2}\cos(k_0\eta)+u_{x0}\ , \tag{9a}$$

$$u_y=\frac{a_0}{\sqrt{2}}(1-\delta_p)^{1/2}\sin(k_0\eta)+u_{y0}\ , \tag{9b}$$

$$u_z=\frac{1}{2h_0}\left\{h_0^2-1-\left[\frac{a_0}{\sqrt{2}}(1+\delta_p)^{1/2}\cos(k_0\eta)+u_{x0}\right]^2-\left[\frac{a_0}{\sqrt{2}}(1-\delta_p)^{1/2}\sin(k_0\eta)+u_{y0}\right]^2\right\}\ . \tag{9c}$$

Hence,

$$x(\eta)=x_0+\beta_{1x}\eta+\frac{r_1}{\sqrt{2}}(1+\delta_p)^{1/2}\sin(k_0\eta)\ , \tag{10a}$$

$$y(\eta)=y_0+\beta_{1y}\eta-\frac{r_1}{\sqrt{2}}(1-\delta_p)^{1/2}\cos(k_0\eta)\ , \tag{10b}$$

$$z(\eta)=z_0+\beta_{1z}\eta-\frac{r_1\beta_{1x}}{\sqrt{2}}(1+\delta_p)^{1/2}\sin(k_0\eta)+\frac{r_1\beta_{1y}}{\sqrt{2}}(1-\delta_p)^{1/2}\cos k_0\eta-z_2\delta_p\sin(2k_0\eta)\ , \tag{10c}$$

where (x_0,y_0,z_0) are related to the initial position of the electron and additional terms of order λ_0/L_0 have been neglected, where L_0 is the laser pulse length. In the above equations,

$$r_1=a_0/h_0k_0\ , \tag{11a}$$

$$z_2=a_0^2/8h_0^2k_0\ , \tag{11b}$$

$$\beta_{1x}=u_{x0}/h_0=\beta_{x0}/(1+\beta_{z0})\ , \tag{11c}$$

$$\beta_{1y}=u_{y0}/h_0=\beta_{y0}/(1+\beta_{z0})\ , \tag{11d}$$

$$\beta_{1z}=\frac{h_0^2-(1+a_0^2/2+u_{10}^2)}{2h_0^2}\ . \tag{11e}$$

Notice that for either circular ($\delta_p=0$) or linear ($\delta_p=1$) polarization, the average components of the electron momentum $\bar{u}_x,\bar{u}_y,\bar{u}_z$ (averaged over a laser period), and the average axial electron velocity, $\bar{\beta}_z=\bar{v}_z/c$, are given by

$$\bar{u}_x=u_{x0}\ , \tag{12a}$$

$$\bar{u}_y=u_{y0}\ , \tag{12b}$$

$$\bar{u}_z=u_{z0}-a_0^2/4h_0\ , \tag{12c}$$

$$\bar{\beta}_z=\frac{\beta_{z0}-a_0^2/4\gamma_0h_0}{1+a_0^2/4\gamma_0h_0}\ . \tag{12d}$$

Hence, the axial momentum of the electron beam is reduced as a result of its interaction with the laser field. This is due to the ponderomotive force associated with the front of the laser pulse [2,35]. This implies that the angle at which the electron beam is propagating with respect to the z axis (i.e., the laser-electron beam interaction angle) is modified by the presence of the laser. In terms of the average components of the electron momentum, the laser-electron beam interaction angle θ_I, defined as the angle between the z axis and the average direction of the electron beam (while it is within the laser field), is given by

$$\cos\theta_I=\bar{u}_z/(u_{x0}^2+u_{y0}^2+\bar{u}_z^2)^{1/2}\ . \tag{13}$$

Although this change in direction is generally small, it is important: the scattered radiation will occur in a narrow cone centered about the direction of the electron beam within the laser field, and not about the initial direction of the electron beam.

III. COORDINATE TRANSFORMATIONS

The coordinate system (x,y,z) used in the previous section was defined in reference to the incident laser field. The electron beam, as it interacts with the laser field, is moving at some angle θ_I with respect to the z axis, where θ_I is given by Eq. (13). Since the scattered radiation will emerge in a narrow cone about the direction of the electron beam, it is convenient to introduce a new coordinate system (x',y',z'), such that the electron beam is propagating along the z' axis; then $\mathbf{e}_z\cdot\mathbf{e}_{z'}=\cos\theta_I$, where $\mathbf{e}_{z,z'}$ are unit vectors in the z and z' directions. In terms of the coordinate system (x,y,z), the direction of propagation of the electron beam is given by $\bar{u}\mathbf{e}_{z'}=\bar{u}_x\mathbf{e}_x+\bar{u}_y\mathbf{e}_y+\bar{u}_z\mathbf{e}_z$, where $\bar{u}^2=\bar{u}_x^2+\bar{u}_y^2+\bar{u}_z^2$. The unit vector $\mathbf{e}_{x'}$ is chosen to reside in the (x,z) plane, which is the plane of polarization for the case of linear polarization (i.e., when $\delta_p=1$ the electric field is in the x direction). The relationship between the coordinate systems is shown in Fig. 1. Assuming that the electron beam axis is in the first quadrant of the (x,y,z) plane, i.e., $\bar{u}_x,\bar{u}_y,\bar{u}_z>0$, the unit vectors transform according to

$$\mathbf{e}_{x'}=l_1\mathbf{e}_x+m_1\mathbf{e}_y+n_1\mathbf{e}_z\ , \tag{14a}$$

$$\mathbf{e}_{y'}=l_2\mathbf{e}_x+m_2\mathbf{e}_y+n_2\mathbf{e}_z\ , \tag{14b}$$

$$\mathbf{e}_{z'}=l_3\mathbf{e}_x+m_3\mathbf{e}_y+n_3\mathbf{e}_z\ . \tag{14c}$$

The transform coefficients can be expressed in terms of the rotation angles θ_I and ν, where ν is the angle between the x and x' axes ($\mathbf{e}_x\cdot\mathbf{e}_{x'}=\cos\nu$),

$$l_1=\cos\nu\ , \tag{15a}$$

$$l_2=-\sin(\nu)(1-\cos^2\theta_I/\cos^2\nu)^{1/2}\ , \tag{15b}$$

$$l_3=\tan\nu\cos\theta_I\ , \tag{15c}$$

$$m_1=0\ , \tag{15d}$$

$$m_2=\cos\theta_I/\cos\nu\ , \tag{15e}$$

$$m_3=(1-\cos^2\theta_I/\cos^2\nu)^{1/2}\ , \tag{15f}$$

$$n_1=-\sin\nu\ , \tag{15g}$$

$$n_2=-\cos(\nu)(1-\cos^2\theta_I/\cos^2\nu)^{1/2}\ , \tag{15h}$$

$$n_3=\cos\theta_I\ . \tag{15i}$$

These coefficients could also be written in terms of the components of average electron momentum by noting that $\cos\theta_I=\bar{u}_z/\bar{u}$ and $\cos\nu=\bar{u}_z/(\bar{u}_x^2+\bar{u}_z^2)^{1/2}$. For circular polarization, the (x,y) symmetry of the laser field allows us to choose our coordinate system so that $\bar{u}_y=u_{y0}=0$. In that case, $\nu=\theta_I$, and the above expressions simplify considerably.

In this new coordinate system, the average electron motion is in the z' direction, and the electron executes periodic motion in (x',y',z'), which depends on the incident angle and the laser polarization. Since the scattered radiation will emerge in a narrow cone about the direction of the electron's average (relativistic) motion, it is convenient to introduce the spherical coordinates (r,θ,ϕ) (with θ measured from the z' axis and ϕ measured from the x' axis) to perform the calculation of the radiation pattern (Sec. IV). This coordinate system is related to the (x',y',z') system through the usual transforms $x'=r\sin\theta\cos\phi$, $y'=r\sin\theta\sin\phi$, $z'=r\cos\theta$; the unit vectors $(\mathbf{e}_r,\mathbf{e}_\theta,\mathbf{e}_\phi)$ are given by

$$\mathbf{e}_r=\sin\theta\cos\phi\mathbf{e}_{x'}+\sin\theta\sin\phi\mathbf{e}_{y'}+\cos\theta\mathbf{e}_{z'}\ , \tag{16a}$$

$$\mathbf{e}_\theta=\cos\theta\cos\phi\mathbf{e}_{x'}+\cos\theta\sin\phi\mathbf{e}_{y'}-\sin\theta\,\mathbf{e}_{z'}\ , \tag{16b}$$

$$\mathbf{e}_\phi=-\sin\phi\mathbf{e}_{x'}+\cos\phi\mathbf{e}_{y'}\ , \tag{16c}$$

These can further be related to the unit vectors $(\mathbf{e}_x,\mathbf{e}_y,\mathbf{e}_z)$ using the transformations of Eq. (14). It is useful to explicitly write out the relation for $\mathbf{e}_r$, because it provides an opportunity to define quantities used in Sec. IV:

$$\mathbf{e}_r=\Omega_x\mathbf{e}_x+\Omega_y\mathbf{e}_y+(\Omega_z-1)\mathbf{e}_z \tag{17}$$

where

$$\Omega_x=l_1\sin\theta\cos\phi+l_2\sin\theta\sin\phi+l_3\cos\theta\ , \tag{18a}$$

$$\Omega_y=m_1\sin\theta\cos\phi+m_2\sin\theta\sin\phi+m_3\cos\theta\ , \tag{18b}$$

$$\Omega_z=1+n_1\sin\theta\cos\phi+n_2\sin\theta\sin\phi+n_3\cos\theta\ . \tag{18c}$$

The reason for the form of the definition of Ω_z will become clear in Sec. IV.

IV. SCATTERED RADIATION

The energy spectrum of the radiation emitted by a single electron in an arbitrary orbit $\mathbf{r}(t)$ and $\boldsymbol{\beta}(t)$ can be calculated from the Lienard-Wiechert potentials [36],

$$\frac{d^2I}{d\omega\,d\Omega}=\frac{e^2\omega^2}{4\pi^2c}\left|\int_{-T/2}^{T/2}dt[\mathbf{n}\times(\mathbf{n}\times\boldsymbol{\beta})]\times\exp[i\omega(t-\mathbf{n}\cdot\mathbf{r}/c)]\right|^2\ , \tag{19}$$

where $d^2I/d\omega\,d\Omega$ is the energy radiated per frequency ω per solid angle Ω during the interaction time T and $\mathbf{n}$ is a unit vector pointing in the direction of observation. This expression can be evaluated using standard classical techniques; we follow the general approach used in previous analyses of Thomson scattering in a counterpropagating geometry [1,2], and by several authors in an analysis of undulator radiation [23–29].

The scattered radiation will be polarized in the direction of $\mathbf{n}\times(\mathbf{n}\times\boldsymbol{\beta})$, where $\mathbf{n}=\mathbf{e}_r$ and $\mathbf{n}\times(\mathbf{n}\times\boldsymbol{\beta})=-\boldsymbol{\beta}\cdot\mathbf{e}_\theta-\boldsymbol{\beta}\cdot\mathbf{e}_\phi$. Hence, the scattered intensity can be written as $I=I_\theta+I_\phi$, where I_θ and I_ϕ are the intensities of radiation with polarizations in the $\mathbf{e}_\theta$ and $\mathbf{e}_\phi$ directions, respectively. Using the relation $c\beta\,dt=(d\mathbf{r}/d\eta)d\eta$, and identifying the phase $\psi=\omega(t-\mathbf{n}\cdot\mathbf{r}/c)$, Eq. (19) can be written as $d^2I/d\omega\,d\Omega=d^2I_\theta/d\omega\,d\Omega+d^2I_\phi/d\omega\,d\Omega$, where

$$\frac{d^2I_\theta}{d\omega\,d\Omega}=\frac{e^2\omega^2}{4\pi^2c^3}\left|\int_{-\eta_0}^{\eta_0}d\eta\left[\frac{d\mathbf{r}}{d\eta}\cdot\mathbf{e}_\theta\right]\exp(i\psi)\right|^2\ , \tag{20a}$$

$$\frac{d^2I_\phi}{d\omega\, d\Omega}=\frac{e^2\omega^2}{4\pi^2c^3}\left|\int_{-\eta_0}^{\eta_0}d\eta\left[\frac{d\mathbf{r}}{d\eta}\cdot\mathbf{e}_\phi\right]\exp(i\psi)\right|^2 . \quad (20b)$$

The integration is now over the independent variable $\eta=z+ct$, with limits of integration $\eta_0=(1+\bar{\beta}_z)cT/2$, where $\bar{\beta}_z$ is the average axial electron velocity given by Eq. (12d); Eqs. (20) can also be written solely in terms of the phase by noting that $-k(d\mathbf{r}/d\eta)\cdot\mathbf{e}_\theta=(\partial^2\psi/\partial\theta\partial\eta)$ and $-k(d\mathbf{r}/d\eta)\cdot\mathbf{e}_\phi=(\partial^2\psi/\partial\phi\partial\eta)_{\theta=\pi/2}$. The phase can be expressed in terms of the electron trajectory $x(\eta),y(\eta),z(\eta)$ using the transformation coefficients $\Omega_x,\Omega_y,\Omega_z$,

$$\psi=k\eta-k[\Omega_x x(\eta)+\Omega_y y(\eta)+\Omega_z z(\eta)] . \quad (21)$$

We now calculate the intensity distributions of emitted radiation for the cases of circularly polarized and linearly polarized laser light, using the electron trajectories given in Eqs. (10) with values of δ_p of 0 and 1, respectively.

A. Circular polarization

For circular polarization ($u_{y0}=0$ and $\nu=\theta_I$), using the trajectories in Eqs. (10a)–(10c) and $\delta_p=0$, the phase can be written in the form

$$\psi=\psi_0+kg\eta-b_s\sin k_0\eta+b_c\cos k_0\eta , \quad (22)$$

where

$$\psi_0=-k(\Omega_x x_0+\Omega_y y_0+\Omega_z z_0) , \quad (23a)$$

$$g=1-\Omega_x\beta_{1x}-\Omega_y\beta_{1y}-\Omega_z\beta_{1z}$$
$$=1-(1+\cos\theta/\cos\theta_I)\beta_{1z} , \quad (23b)$$

$$b_s=kr_1(\Omega_x-\Omega_z\beta_{1x})/\sqrt{2}$$
$$=(kr_1/\sqrt{2})[\cos\theta\sin(\theta_I)(1-\beta_{1z})-\beta_{1x}$$
$$+\sin\theta\cos(\phi)(\cos\theta_I+\beta_{1x}\sin\theta_I)] , \quad (23c)$$

$$b_c=kr_1(\Omega_y-\Omega_z\beta_{1y})/\sqrt{2}$$
$$=(kr_1/\sqrt{2})\sin\theta\sin\phi . \quad (23d)$$

Here, the orbit parameters r_1, β_{1x}, and β_{1z} are given by Eqs. (11a), (11c), and (11e).

The spectrum of scattered radiation can be found by calculating the integrals:

$$I_0=\int_{-\eta_0}^{\eta_0}d\eta\exp(i\psi)$$
$$=e^{i\psi_0}\sum_{n,m}\frac{\sin\bar{k}\eta_0}{\bar{k}}2J_m(b_c)J_{n+m}(b_s)e^{im\pi/2} , \quad (24a)$$

$$I_c=\int_{-\eta_0}^{\eta_0}d\eta\cos(k_0\eta)\exp(i\psi)$$
$$=e^{i\psi_0}\sum_{n,m}\frac{\sin\bar{k}\eta_0}{\bar{k}}J_m(b_c)[J_{n+m+1}(b_s)$$
$$+J_{n+m-1}(b_s)]e^{im\pi/2} , \quad (24b)$$

$$I_s=\int_{-\eta_0}^{\eta_0}d\eta\sin(k_0\eta)\exp(i\psi)$$
$$=e^{i\psi_0}\sum_{n,m}\frac{\sin\bar{k}\eta_0}{\bar{k}}J_m(b_c)[J_{n+m+1}(b_s)$$
$$-J_{n+m-1}(b_s)]e^{i(m-1)\pi/2} , \quad (24c)$$

where $\bar{k}=kg-nk_0$. The summations in the above expressions can be simplified by using Graf's addition theorem [37]

$$\sum_{m=-\infty}^{\infty}J_m(b_c)J_{n+m}(b_s)e^{im\pi/2}=J_n(b_t)(b_s+ib_c)^n/b_t^n , \quad (25)$$

where $b_t^2=b_s^2+b_c^2$. Using the recursion relations $J_{n+1}+J_{n-1}=2nJ_n/b_t$ and $J_{n+1}-J_{n-1}=-2J_n'$, the radiation spectrum for the n harmonic can be written as

$$\frac{d^2I_n}{d\omega\, d\Omega}=\frac{e^2k_0^2}{\pi^2c}\left[\frac{\sin\bar{k}\eta_0}{\bar{k}}\right]^2[A_1J_n^2+A_2(J_n'/b_t)^2] , \quad (26a)$$

where

$$A_1=\left[\frac{k}{k_0}\frac{\partial g}{\partial\theta}-\frac{n}{2b_t^2}\frac{\partial b_t^2}{\partial\theta}\right]^2$$
$$+\frac{n^2}{b_t^4}\left[b_s\left[\frac{\partial b_s}{\partial\phi}\right]_{\theta=\pi/2}+b_c\left[\frac{\partial b_c}{\partial\phi}\right]_{\theta=\pi/2}\right]^2 , \quad (26b)$$

$$A_2=\left[b_c\frac{\partial b_s}{\partial\theta}-b_s\frac{\partial b_c}{\partial\theta}\right]^2$$
$$+\left[b_c\left[\frac{\partial b_s}{\partial\phi}\right]_{\theta=\pi/2}-b_s\left[\frac{\partial b_c}{\partial\phi}\right]_{\theta=\pi/2}\right]^2 , \quad (26c)$$

and $J_n=J_n(b_t)$. We discuss the features of the spectra, and show plots of specific examples, in Sec. V.

In the backscattered direction, i.e., along the z' axis, the above expressions simplify considerably. For $\theta=0$, the arguments become $b_c=0$ and $b_t=b_s$; the backscattered spectrum can then be written as

$$\frac{d^2I_n(\theta=0)}{d\omega\, d\Omega}=\frac{e^2k^2}{\pi^2c}\left[\frac{\sin\bar{k}\eta_0}{\bar{k}}\right]^2\left[\frac{a_0^2}{2h_0^2}\right]$$
$$\times[(J_n')^2+(\cos\theta_I+\beta_{1x}\sin\theta_I)^2$$
$$\times(nJ_n/b_s)^2] , \quad (27)$$

where $b_s\approx(na_0/\sqrt{2}h_0)\sin\theta_I$ if k is taken to be its resonant value, $k\approx nk_0/g=nk_0/[1-(1+\cos\theta/\cos\theta_I)\beta_{1z}]$. Furthermore, when $b_s^2\ll1$, Eq. (27) will be dominated by the fundamental, i.e., $J_1'\approx\frac{1}{2}$ and $J_I\approx b_s/2$. In the limit $\theta_I=0$ (head-on scattering), $b_s=0$, and only the fundamental, $n=1$, is nonzero. In this limit, the term in the square brackets in Eq. (26) is equal to $\frac{1}{2}$, and we recover the result obtained previously for backscattered radiation in a head-on geometry [1].

B. Linear polarization

For linear polarization, the rotation angles θ_I and ν are defined by Eqs. (13) and (15), and the phase can be written as

$$\psi=\psi_0+kg\eta-b_1\sin k_0\eta+b_2\sin 2k_0\eta\ , \tag{28}$$

where ψ_0 and g are given by Eqs. (23a) and (23b),

$$\begin{aligned} b_1&=kr_1(\Omega_x-\Omega_z\beta_{1x})\\ &=kr_1[(l_1-\beta_{1x}n_1)\sin\theta\cos\phi+(l_2-\beta_{1x}n_2)\sin\theta\cos\phi\\ &\quad+(l_3-\beta_{1x}n_3)\cos\theta-\beta_{1x}]\ , \end{aligned} \tag{29a}$$

$$\begin{aligned} b_2&=k\Omega_z z_2\\ &=kz_2(1+n_1\sin\theta\cos\phi+n_2\sin\theta\sin\phi+n_3\cos\theta)\ . \end{aligned} \tag{29b}$$

Here, the orbit parameters r_1, β_{1x}, and z_2 are given by Eqs. (11a), (11c), and (11e), and the transformation coefficients (l,m,n) are given by Eqs. (15a)–(15i). To calculate the spectrum, it is necessary to evaluate the integrals

$$\begin{aligned} I_0&=\int_{-\eta_0}^{\eta_0}d\eta\exp(i\psi)\\ &=e^{i\psi_0}\sum_{n,m}\frac{\sin\bar{k}\eta_0}{\bar{k}}2J_m(b_2)J_{n+2m}(b_1)\ , \end{aligned} \tag{30a}$$

$$\begin{aligned} I_1&=\int_{-\eta_0}^{\eta_0}d\eta\cos(k_0\eta)\exp(i\psi)\\ &=e^{i\psi_0}\sum_{n,m}\frac{\sin\bar{k}\eta_0}{\bar{k}}J_m(b_2)\\ &\quad\times[J_{n+2m+1}(b_1)+J_{n+2m-1}(b_1)]\ , \end{aligned} \tag{30b}$$

$$\begin{aligned} I_2&=\int_{-\eta_0}^{\eta_0}d\eta\cos(2k_0\eta)\exp(i\psi)\\ &=e^{i\psi_0}\sum_{n,m}\frac{\sin\bar{k}\eta_0}{\bar{k}}J_m(b_2)\\ &\quad\times[J_{n+2m+2}(b_1)+J_{n+2m-2}(b_1)]\ , \end{aligned} \tag{30c}$$

where $\bar{k}=gk-nk_0$. Using these results, the spectrum can be written as

$$\begin{aligned} \frac{d^2I_{\theta n}}{d\omega\,d\Omega}&=\frac{e^2k_0^2}{4\pi^2c}\left[\frac{\sin\bar{k}\eta_0}{\bar{k}}\right]^2\\ &\quad\times\left[\frac{k}{k_0}\frac{\partial g}{\partial\theta}B_0-\left[\frac{\partial b_1}{\partial\theta}\right]B_1+2\left[\frac{\partial b_2}{\partial\theta}\right]B_2\right]^2\ , \end{aligned} \tag{31a}$$

$$\begin{aligned} \frac{d^2I_{\phi n}}{d\omega\,d\Omega}&=\frac{e^2k_0^2}{4\pi^2c}\left[\frac{\sin\bar{k}\eta_0}{\bar{k}}\right]^2\\ &\quad\times\left[\left[\frac{\partial b_1}{\partial\phi}\right]_{\phi=\pi/2}B_1-2\left[\frac{\partial b_2}{\partial\phi}\right]_{\phi=\pi/2}B_2\right]^2\ , \end{aligned} \tag{31b}$$

where

$$B_0=\sum_{m=-\infty}^{\infty}2J_m(b_2)J_{n+2m}(b_1)\ , \tag{32a}$$

$$B_1=\sum_{m=-\infty}^{\infty}J_m(b_2)[J_{n+2m+1}(b_1)+J_{n+2m-1}(b_1)]\ , \tag{32b}$$

$$B_2=\sum_{m=-\infty}^{\infty}J_m(b_2)[J_{n+2m+2}(b_1)+J_{n+2m-2}(b_1)]\ . \tag{32c}$$

We discuss the features of the spectra, and show plots of specific examples, in Sec. V.

The general expression for the spectrum of backscattered radiation, i.e., in the direction $\theta=0$, is given by

$$\begin{aligned} \frac{d^2I_n(\theta=0)}{d\omega\,d\Omega}&=\frac{e^2k^2}{4\pi^2c}\left[\frac{\sin\bar{k}\eta_0}{\bar{k}}\right]^2\left[\frac{a_0^2}{h_0^2}\right]\frac{1}{\beta_1^2}\\ &\quad\times\left\{[\beta_{1y}^2+\beta_{1z}^2+\beta_{1x}^2(2\beta_{1z}+\beta_{1x}^2+\beta_{1y}^2)]B_1^2\right.\\ &\quad+\left[\frac{a_0^2}{16h_0^2}\right](\beta_{1x}^2+\beta_{1y}^2)B_2^2\\ &\quad\left.+\left[\frac{a_0}{2h_0}\right]\beta_{1x}(\beta_{1z}+\beta_{1x}^2+\beta_{1y}^2)B_1B_2\right\}\ , \end{aligned} \tag{33}$$

where the arguments of the Bessel functions are $b_1=nk_0r_1\beta_{1x}/\beta_1$ and $b_2=kz_2(1+\beta_{1z}/\beta_1)$, the resonant wave number is $k=nk_0/(1-\beta_{1z}-\beta_1)$, $\beta_1^2=\beta_{1x}^2+\beta_{1y}^2+\beta_{1z}^2$ and $\beta_{1x,y,z}$ are given by Eqs. (11c)–(11e).

It is possible to gain some insight into the radiation patterns by examining the backscattered spectrum for three different interaction geometries: head-on scattering in which the laser and electron beams are colinear ($\theta_I=0$, $\beta_1=\beta_{1z}$, and $\beta_{1x}=\beta_{1y}=0$); transverse scattering in which the electron beam is normal to the plane of the laser polarization ($\theta_I=\pi/2$, $\beta_1=\beta_{1y}$, and $\beta_{1x}=\beta_{1z}=0$); transverse scattering in which the electron beam is in the plane of the laser polarization ($\theta_I=\pi/2$, $\beta_1=\beta_{1x}$, and $\beta_{1y}=\beta_{1z}=0$).

For head-on scattering, the arguments of the Bessel functions become $b_1=0$, $b_2=2kz_2$, and Eq. (33) reduces to

$$\frac{d^2I_n(\theta=0)}{d\omega\,d\Omega}=\frac{e^2k^2}{4\pi^2c}\left[\frac{\sin\bar{k}\eta_0}{\bar{k}}\right]^2\left[\frac{a_0^2}{h_0^2}\right]B_1^2\ , \tag{34a}$$

where

$$B_1^2=[J_{(n+1)/2}(b_2)-J_{(n-1)/2}(b_2)]^2 \tag{34b}$$

and $k=nk_0/(1-2\beta_1)$. Note that only odd harmonics are generated, and that we recover the previous result for colinear scattering [1].

Now consider transverse scattering in which the electron beam is normal to the laser plane ($\beta_1=\beta_{1y}$). For this case, $b_1=0$, $b_2=kz_2$, and Eq. (33) becomes

$$\frac{d^2I_n(\theta=0)}{d\omega\, d\Omega}=\frac{e^2k^2}{4\pi^2c}\left[\frac{\sin\bar{k}\eta_0}{\bar{k}}\right]^2\left[\frac{a_0^2}{h_0^2}\right]\times\left[B_1^2+\left[\frac{a_0^2}{16h_0^2}\right]B_2^2\right], \tag{35a}$$

where

$$B_1^2=[J_{(n+1)/2}(b_2)-J_{(n-1)/2}(b_2)]^2, \tag{35b}$$

$$B_2^2=[J_{(n+2)/2}(b_2)+J_{(n-2)/2}(b_2)]^2, \tag{35c}$$

and $k=nk_0/(1-\beta_1)$. Both odd and even harmonics are generated, with B_1^2 describing the odd harmonics and B_2^2 describing the even harmonics.

The most complicated of the three cases is that of transverse scattering in which the electron beam is in the plane of polarization ($\beta_1=\beta_{1x}$). Then b_1 does not vanish, and hence the Bessel function sums do not collapse. In this case, $b_1=nk_0r_1$, $b_2=kz_2$, and

$$\frac{d^2I_n(\theta=0)}{d\omega\, d\Omega}=\frac{e^2k^2}{4\pi^2c}\left[\frac{\sin\bar{k}\eta_0}{\bar{k}}\right]^2\left[\frac{a_0^2}{h_0^2}\right]\times\left[\beta_1B_1+\left[\frac{a_0}{4h_0}\right]B_2\right]^2, \tag{36}$$

where $k=nk_0/(1-\beta_1)$. B_1 and B_2 are given by the full summations in Eqs. (32), and both odd and even harmonics appear on-axis.

C. Resonance function

The frequency of the scattered radiation is primarily determined by the resonance function $R_n(k,nk_0)$, where

$$R_n(k,nk_0)=\left[\frac{\sin\bar{k}\eta_0}{\bar{k}\eta_0}\right]^2. \tag{37}$$

This function is sharply peaked at $\bar{k}\eta_0=0$ (i.e., $k[1-(1+\cos\theta/\cos\theta_I)\beta_{1z}]-nk_0=0$), which corresponds to a resonant frequency

$$\omega_n=\frac{n\omega_0}{1-(1+\cos\theta/\cos\theta_I)\beta_{1z}}. \tag{38}$$

The denominator represents a generalized Doppler upshift factor. Note that with this choice of coordinate systems, with $\theta=0$ along the center of the radiation cone, Eq. (38) is independent of ϕ.

The resonant frequency depends upon the interaction angle, the observation angle, the electron energy, and the laser intensity. Equation (38) indicates that the frequency of the scattered radiation is maximum when $\theta=0$, i.e., along the direction of the electron beam within the laser field. $\omega_1(\theta)$ (the resonant frequency of the first harmonic) is plotted in Fig. 2 for $a_0=2$ and three different interaction angles, $\theta_I=0°$, 60°, and 90°. The frequency is plotted

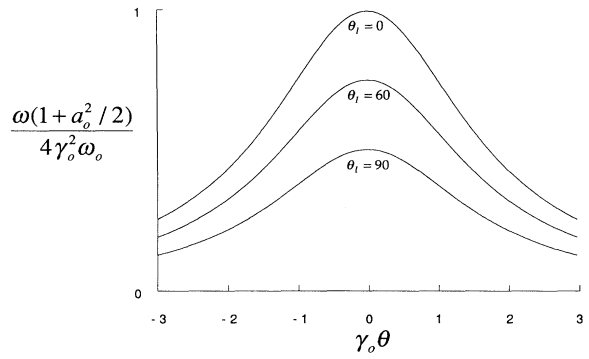

FIG. 2. The frequency of radiation into the fundamental ($n=1$) as a function of observation angle. Resonance contours, $\omega(\theta)$, are shown for three different interaction angles, $\theta_I=0°$, 60°, and 90°. The frequency is plotted in dimensionless units, $\omega/[4\gamma_0^2\omega_0/(1+a_0^2/2)]$ ($4\gamma_0^2\omega_0$ is the frequency of the fundamental along $\theta=0$ in the low a_0 limit); the observation angle is plotted in units of $\gamma_0\theta$.

in units of $4\gamma_0^2\omega_0/(1+a_0^2/2)$, the frequency of the fundamental along $\theta=0$. Increasing θ_I decreases the frequency of a given harmonic.

In the limits $\gamma_0^2\gg a_0^2$, $\beta_0\sim1$, and $\theta^2\ll1$, the resonant frequency can be written as

$$\omega_n=\frac{2(1+\beta_{z0})\gamma_0^2n\omega_0}{(1+a_0^2/2+\gamma_0^2\theta^2)}. \tag{39}$$

Increasing a_0 decreases the frequency of a given harmonic [by a factor $(1+a_0^2/2)$ on-axis]. Also, note that for head-on interactions ($\beta_{z0}\sim1$), the resonant frequency is twice that for transverse interaction geometries ($\beta_{z0}\sim0$). For $a_0^2\ll1$, $\theta_I=0$, and $\theta=0$, Eq. (39) reduces to the familiar result, $\omega_n=4\gamma_0^2n\omega_0$.

The width of the spectrum about ω_n, defined by $\Delta\omega=\int d\omega R_n$, is given by

$$\Delta\omega/\omega_n=1/(nN_0), \tag{40}$$

where $N_0=2\eta_0/\lambda_0$ is the number of periods of the laser field with which the electron interacts. This is sometimes referred to as the intrinsic bandwidth of the scattered radiation. For sufficiently large N_0, the frequency spectra for two different harmonics, n and n', are well separated. This has been assumed in deriving Eqs. (26) and (31), i.e., $(\sum_n R_n^{1/2}F_n)^2\approx\sum_n R_nF_n^2$, where F_n is a function of n. Furthermore, $\Delta\omega^{-1}R_n(k,nk_0)\to\delta(\omega-\omega_n)$ as $N_0\to0$, i.e., the spectral resonance becomes a δ function about the resonant frequency.

Equation (39) also implies that radiation with a bandwidth $\Delta\omega$ about ω_n can be found within a cone half-angle $\Delta\theta$ about $\theta=0$ given by

$$\Delta\theta^2 \approx \frac{(1+a_0^2/2)\Delta\omega}{\gamma_0^2\omega_n} , \tag{41}$$

assuming $\Delta\omega/\omega \ll 1$.

V. RADIATION DISTRIBUTIONS

The expressions derived in Sec. IV describe the spectrum and angular distribution of radiation emitted by a single electron as a result of its interaction with an intense laser field. The radiation is emitted in a narrow ($\sim 1/\gamma$) cone about the forward direction ($\theta=0$). If the laser strength parameter is low, $a_0 < 1$, most of the radiation goes into the fundamental ($n=1$). As a_0 increases, radiation into higher harmonics increases; the harmonics become important when $a_0 > 1$. The intensity distributions below were generated for the case of an electron with relativistic factor $\gamma_0=10$, and linearly and circularly polarized laser pulses with strength parameter $a_0=2$. An electron beam of this energy can be produced by a compact accelerator; a laser of this intensity is near the current state-of-the-art, and is reasonable to expect in the next few years [13].

The plots below show the radiation as viewed by a detector located at z_0', and centered on the z' axis (i.e., the backscattered direction, $\theta=0$, is in the middle of the detector). Because the radiation is confined to a narrow cone, $x'/z_0' \sim \theta$, and $y'/z_0' \sim \theta$; distances from the center of the detector are measured in units of $\gamma_0 x'/z_0'$, $\gamma_0 y'/z_0' \sim \gamma_0\theta$. Assuming the electron sees many laser periods (an excellent assumption for picosecond laser pulses at micron wavelengths, see Sec. VI), the resonance function given by Eq. (37) is a δ function, and the radiation emitted into a particular angle θ is radiation of a particular frequency. This frequency, determined by the resonance condition [Eq. (38), and shown in Fig. 2], is conveyed qualitatively through a color scale applied to the surface plots (the same scale is common to all). Further, in the figures below, the electron is assumed to see the same number of laser periods in each case (for both head-on and transverse interactions); thus, the normaliza-

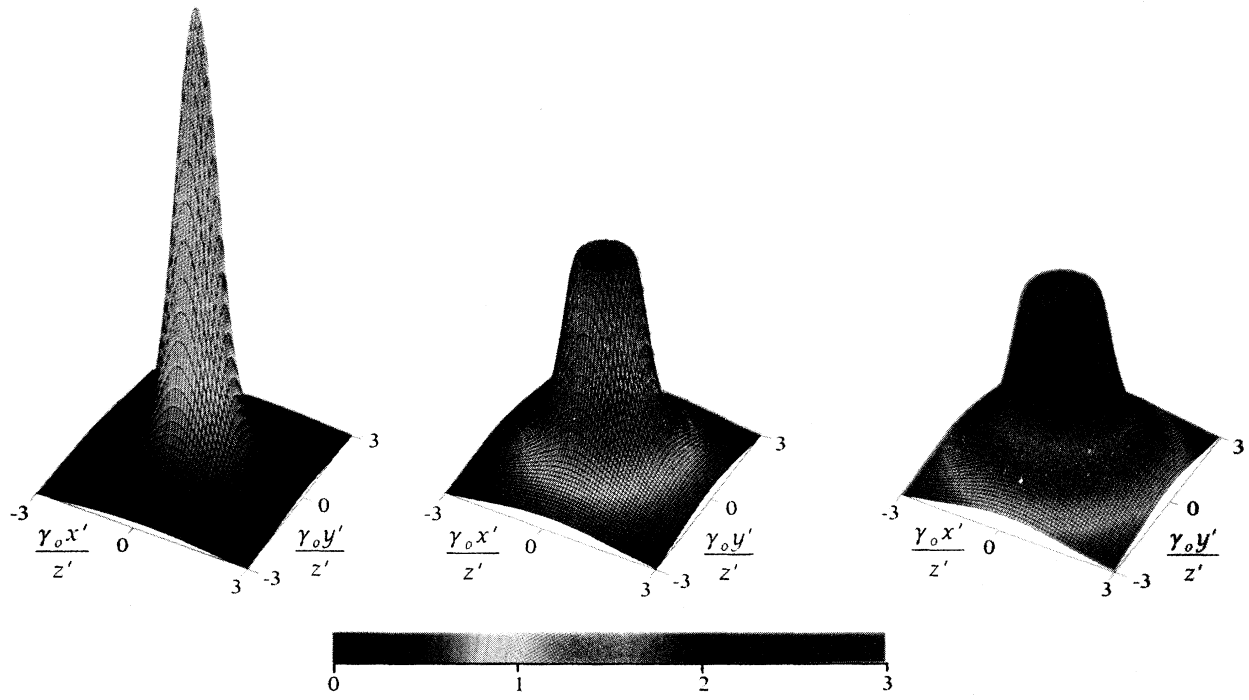

FIG. 3. Circular polarization, head-on scattering. The normalized intensity of radiation scattered by a relativistic electron ($\gamma_0=10$) from a counterpropagating ($\theta_I=0$) high intensity ($a_0=2$) circularly polarized laser pulse, viewed in the plane of a detector. The detector is located at z_0', and centered on the z' axis [backscattered radiation ($\theta=0$) falls on the center of the detector]. Distances in x',y' are measured in units $\gamma_0(x'/z_0')$, $\gamma_0(\gamma'/z_0') \sim \gamma_0\theta$. The three figures show the radiation into the first three harmonics (a) $n=1$; (b) $n=2$; (c) $n=3$. The color scale, marked in units of $4\gamma_0^2\omega_0/(1+a_0^2/2)$, indicates frequency of the scattered radiation.

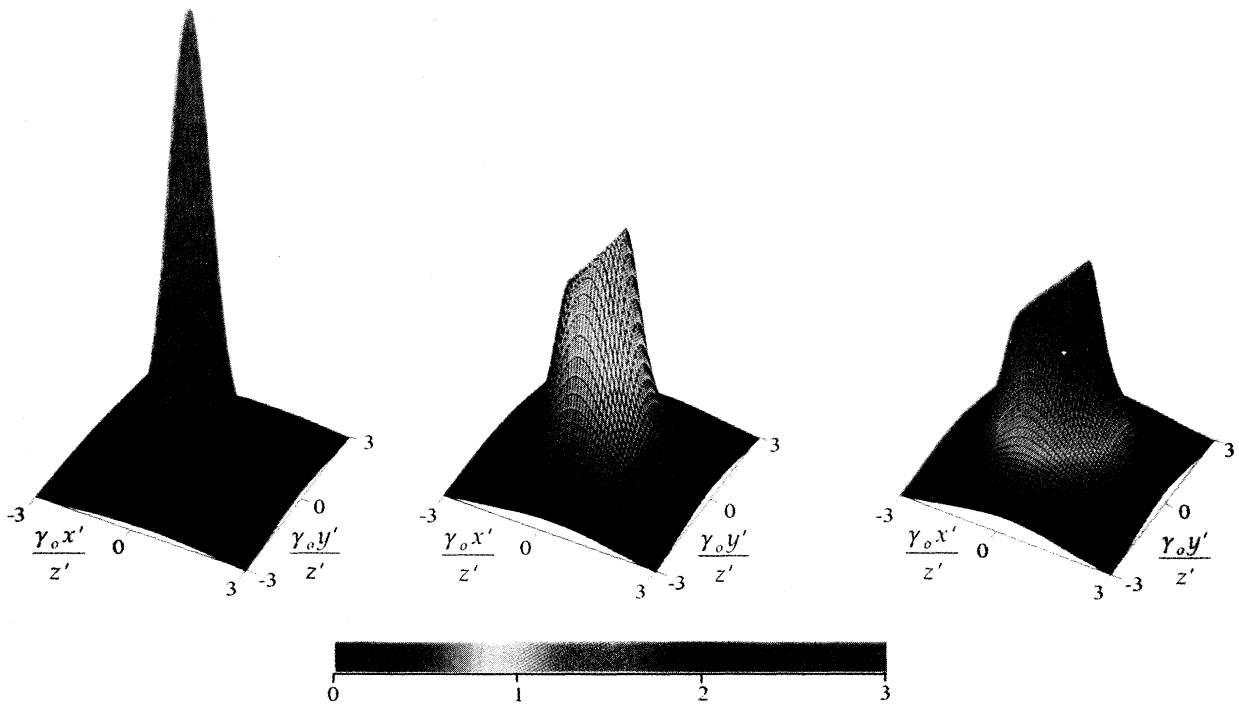

FIG. 4. Circular polarization, transverse scattering. The normalized intensity of radiation scattered by a relativistic electron ($\gamma_0=10$) from a transversely propagating ($\theta_I=90°$), high intensity ($a_0=2$) circularly polarized laser pulse, viewed in the plane of the detector. The detector is centered at z_0' along the z' ($\theta=0$) axis. Distances in x',y' are measured in units $\gamma_0(x'/z_0')$, $\gamma_0(y'/z_0')\sim\gamma_0\theta$. The three figures show radiation into the first three harmonics (a) $n=1$; (b) $n=2$; (c) $n=3$. The color scale, marked in units of $4\gamma_0^2\omega_0/(1+a_0^2/2)$, indicates frequency of the scattered radiation.

tion is the same for all intensity plots (the effect of interaction geometry on photon flux is considered in Sec. VI).

A. Circular polarization

Plots of the normalized intensity distribution of scattered radiation, $dI/d\omega\, d\Omega$, are shown in Figs. 3–5. The first of these, Fig. 3, presents the results for a counterstreaming geometry, in which the electron and the circularly polarized laser pulse meet head-on ($\theta_I=0$). These results were obtained previously [1], and are included here for comparison with the results for off-axis scattering derived in this paper. The figure shows radiation emitted into the first three harmonics. The first harmonic peaks on-axis, the highest frequency radiation in that harmonic is emitted on-axis, and the radiation pattern is symmetric about the axis. This symmetry is expected because the electron trajectory is a helix, and its projection in the x-y plane is a circle. The second and third (and all higher) harmonics vanish on-axis; their radiation patterns are symmetric and independent of ϕ. Note that radiation into the nth harmonic, because it is emitted off-axis, occurs at less than n times the frequency of the first harmonic. For example, the intensity of radiation into the second harmonic peaks at an off-axis angle $\gamma_0\theta\sim0.6$,

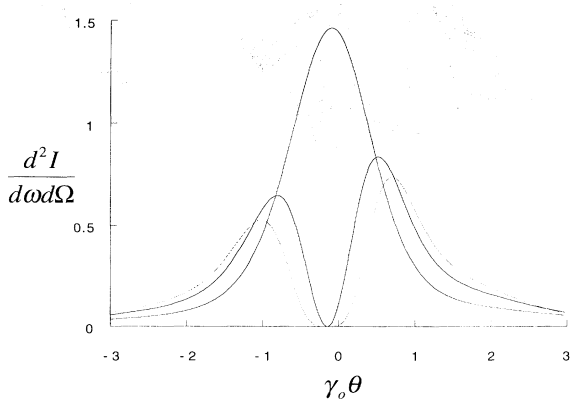

FIG. 5. Circular polarization, transverse scattering. Normalized intensity of the first three harmonics of Fig. 4 along the x' axis of the detector, $a_0=2$, $\gamma_0=10$. Distance along the axis is measured in units of $\gamma_0(x'/z_0')\sim\gamma_0\theta$.

which corresponds to a frequency of $(0.89)(2\omega_1)$, where ω_1 is the frequency of the fundamental on-axis.

The plots in Fig. 4 illustrate the effect of changing the interaction geometry. In particular, they show the intensity distribution, that results when the electron travels at right angles to the laser pulse $\theta_I=90°$. The parameters a_0 and γ_0 are the same as in Fig. 3. The most noticeable difference is in the frequency of the scattered radiation. As the interaction angle is increased toward 90°, a given harmonic peaks at progressively lower frequencies; for example, the frequency of the backscattered radiation in the first harmonic is a factor of 2 lower for transverse geometries [Fig. 4(a)] than for head-on geometries [Fig. 3(a)], a result familiar from inverse Compton scattering.

As the interaction angle is increased from $\theta_I=0°$ to 90°, the trajectory of the electron in its average rest frame changes, increasing in radius and rotating about the y' axis (out of the x'-y' plane). For $\theta_I=90°$, the circle is rotated 45° from the x' axis (i.e., the projection of the motion on the x'-y' plane is an ellipse, and there is also a sinusoidal motion in z'). This displaces the radiation patterns slightly from $\theta=0$ [resulting in some radiation into the harmonics on-axis, Eq. (27)], and introduces ϕ dependence; these effects become more pronounced as a_0 is increased, and some of them are clearly apparent in Fig. 4. The shape of the first harmonic is nearly the same as in the head-on geometry, and it is very slightly displaced in x'; the second and third harmonics show the ϕ dependence, and do not vanish on-axis. The displacement is shown more clearly in Fig. 5, which depicts the intensity in the first three harmonics along the x' axis. The frequency of the radiation at a particular part of this intensity distribution can be estimated more quantitatively by using Figs. 2 and 5 in combination.

B. Linear polarization

Next we consider scattering between a relativistic electron and a linearly polarized laser pulse. Figure 6 illustrates the results, obtained previously [1], for head-on interaction. This figure shows the intensity of radiation into the first three harmonics, again for parameters $a_0=2$, $\gamma_0=10$. The even harmonics vanish on-axis, but the odd harmonics include a peak along $\theta=0$. In general, a particular harmonic n has n peaks. The motion of the electron producing this radiation pattern, when

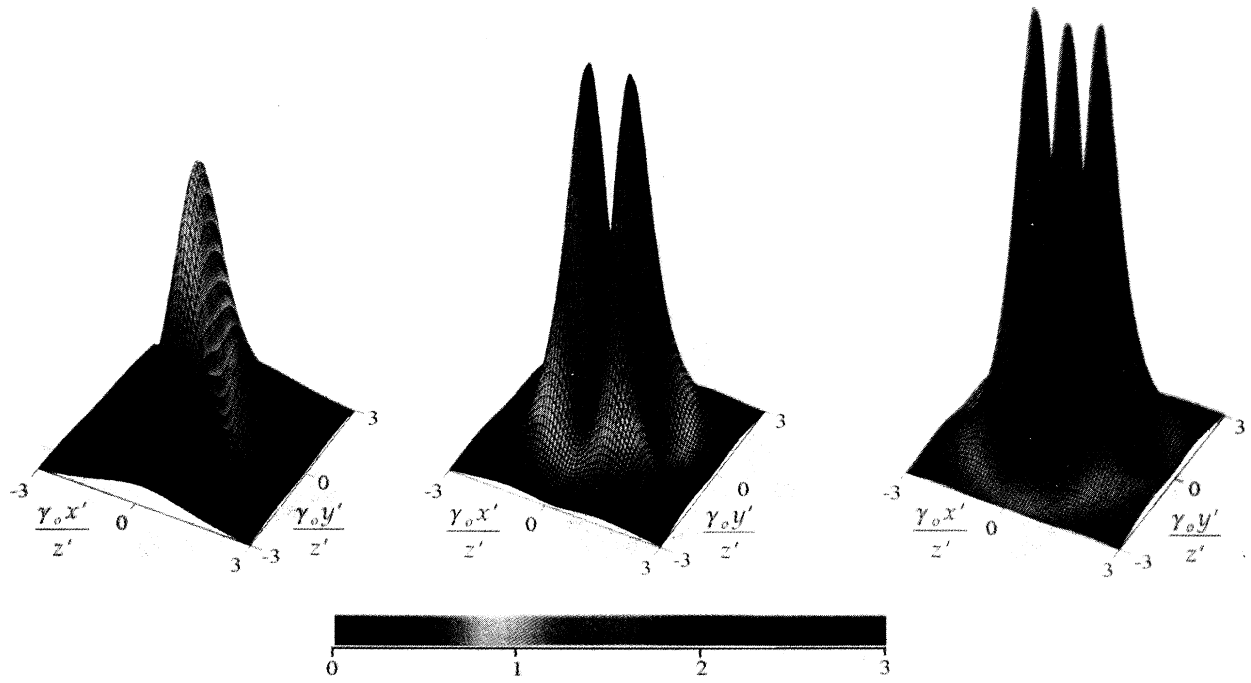

FIG. 6. Linear polarization, head-on scattering. The normalized intensity of radiation scattered by a relativistic electron ($\gamma_0=10$) from a counterpropagating $\theta_I=0$, high intensity ($a_0=2$) linearly polarized laser pulse, viewed in the plane of the detector. The detector is centered at z_0' along the z' ($\theta=0$) axis. Distances in x',y' are measured in units $\gamma_0(x'/z_0')$, $\gamma_0(y'/z_0')\sim\gamma_0\theta$. The three figures show radiation into the first three harmonics (a) $n=1$; (b) $n=2$; (c) $n=3$. The color scale, marked in units of $4\gamma_0^2\omega_0/(1+a_0^2/2)$, indicates frequency of the scattered radiation.

viewed in its average rest frame, is a "figure eight" with its long axis along x', lying in the x'-y' plane. The intensity distribution is thus symmetric in x'. For this value of a_0, harmonics are important; the second and third harmonics are comparable to the fundamental.

We now consider two different classes of off-axis scattering geometries: (1) when the electron is initially traveling in the y-z plane (perpendicular to the plane of polarization); and (2) when the electron is initially traveling in the x-z plane (the plane of polarization). The induced electron trajectories are different for these cases, and result in different radiation patterns.

1. *Electron initially traveling in the y-z plane* ($\beta_{1x}=0$)

When the electron is traveling in the y-z plane, perpendicular to the plane of polarization, the induced trajectory remains a figure eight in the x-z plane. When viewed in the x',y',z' system, as the scattering angle is increased from zero, the figure eight rotates about the x' axis until, when the interaction angle is 90°, the figure eight motion is in the x'-y' plane. Figure 7 shows the radiation emitted into the first three harmonics for $\theta_I=90°$. These plots are quite similar to those of Fig. 6 (head-on geometry). The main difference is in the frequency of the radiation, as described in Eq. (38). Figure 8 shows the intensity of these first three harmonics along the x' axis; this shows that the even harmonics, although small, do not vanish on-axis [see Eq. (35)].

2. *Electron initially traveling in the x-z plane* ($\beta_{1y}=0$)

When the electron is traveling off-axis in the x-z plane (plane of polarization), the induced electron oscillations are no longer symmetric in x'. As the interaction angle is increased from zero, the figure eight (viewed in the x',y',z' system) rotates about the y' axis, and excursions from ($x'=0$, $y'=0$) increase; when the interaction angle reaches 90°, the figure eight is elongated, distorted, and its long axis is rotated 45° from the x' axis, still in the x'-z' plane. Figure 9 displays the radiation patterns for an interaction angle of 90°. The peaks are displaced slightly in x'; more apparent is the asymmetry in the peaks of the second and third harmonics. Figure 10 shows the intensity in the first three harmonics along the x' axis; here the displacement is visible, and it is clear

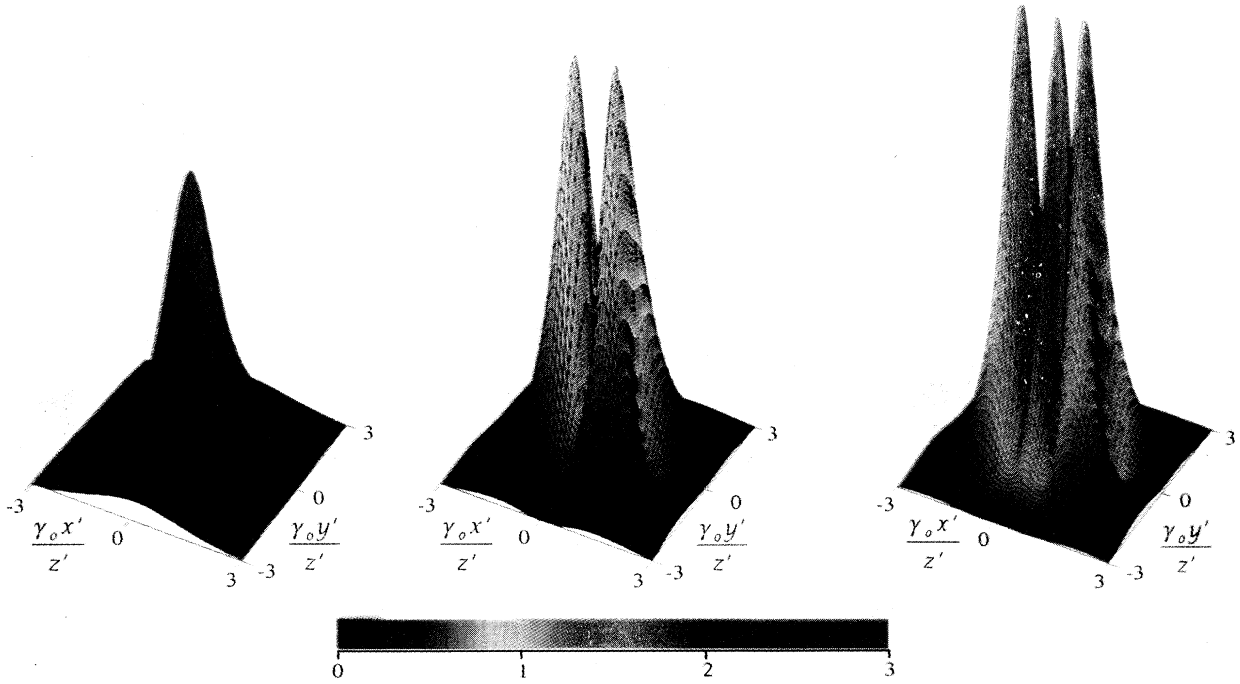

FIG. 7. Linear polarization, transverse scattering ($\beta_{1x}=0$). The normalized intensity of radiation into the first three harmonics emitted by a relativistic electron ($\gamma_0=10$) during interaction with a high intensity ($a_0=2$), linearly polarized laser pulse for an interaction angle of 90°. In this case, the electron is traveling perpendicular to the plane of laser polarization. The detector is centered at z_0' along the z' ($\theta=0$) axis. Distances in x',y' are measured in units $\gamma_0(x'/z_0')$, $\gamma_0(\gamma'/z_0')\sim\gamma_0\theta$. The color scale, marked in units of $4\gamma_0^2\omega_0/(1+a_0^2/2)$, indicates the frequency of the scattered radiation.

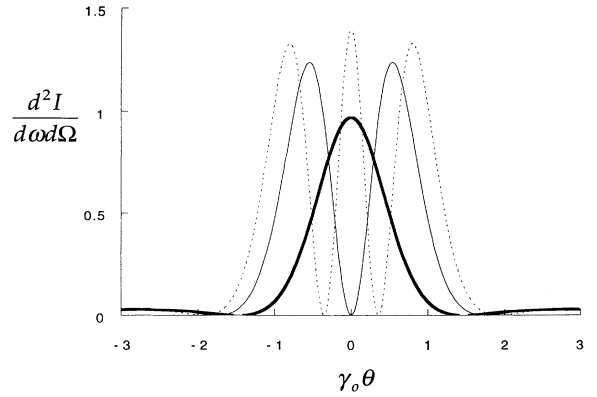

FIG. 8. Linear polarization, transverse scattering, $\beta_{1x}=0$. Normalized intensity of the first three harmonics of Fig. 7 along the x' axis of the detector, $a_0=2$, $\gamma_0=10$. Distance along the axis is measured in units of $\gamma_0(x'/z_0')\sim\gamma_0\theta$.

that the odd harmonics do not peak exactly on-axis and the even harmonics do not vanish on-axis. On-axis, the radiation is described by Eq. (36).

C. Ultrahigh intensity

As the laser strength parameter approaches one, a significant amount of scattered radiation appears in harmonics. When $a_0 \gg 1$, radiation is emitted into many closely spaced harmonics, and the envelope of the spectrum resembles the well-known synchrotron radiation spectrum [1,36]. In fact, if the radiation is from an electron beam rather than a single electron, nonideal effects such as beam emittance and energy spread would cause the harmonics to overlap, producing (in the limit $a_0 \gg 1$) a broadband, continuous spectrum, which extends out to a critical frequency $\omega_c \sim a_0^3$, then falls off rapidly. The asymptotic properties of the radiation spectrum for large a_0 have been analyzed in detail for the case of head-on interaction [1].

Figure 11(a) shows the intensity of the odd harmonics on-axis for the case of a high intensity linearly polarized laser and head-on interaction, as described by Eq. (34). The figure includes plots for $a_0=2$, 4, and 6; harmonic intensity is plotted versus the normalized frequency $\omega/4\gamma^2\omega_0$. This result, obtained previously [1], illustrates the importance of high harmonics for increasingly large a_0. The odd harmonics are closely spaced, the even harmonics vanish on-axis, and the envelope is similar to that for broadband synchrotron radiation. Figure 11(b) shows the effect of off-axis geometries on the harmonic intensity of backscattered radiation, as described by Eq. (35). In particular, it shows the intensity of harmonics along $\theta=0$ for transverse scattering, when the electron motion is in the y-z plane (perpendicular to the plane of polarization).

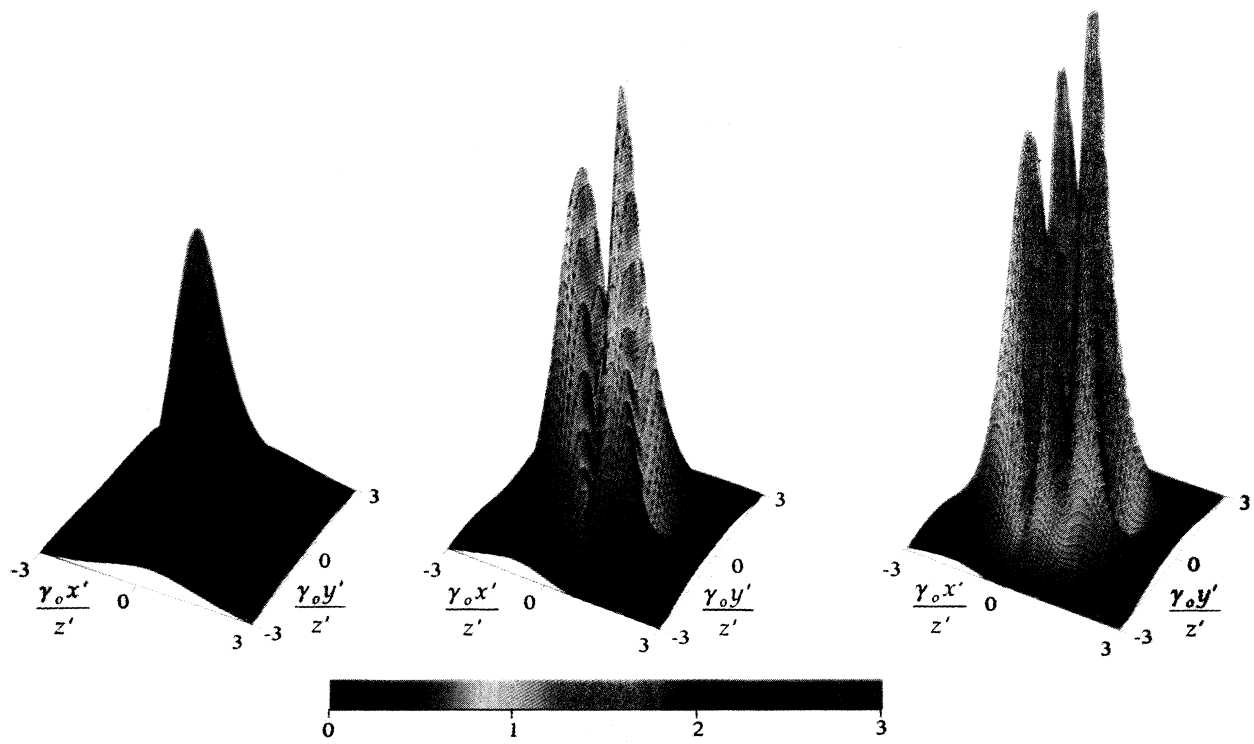

FIG. 9. Linear polarization, transverse scattering, $\beta_{1y}=0$. Same as in Fig. 7, but for the case of the electron traveling in the x-z plane (in the plane of polarization).

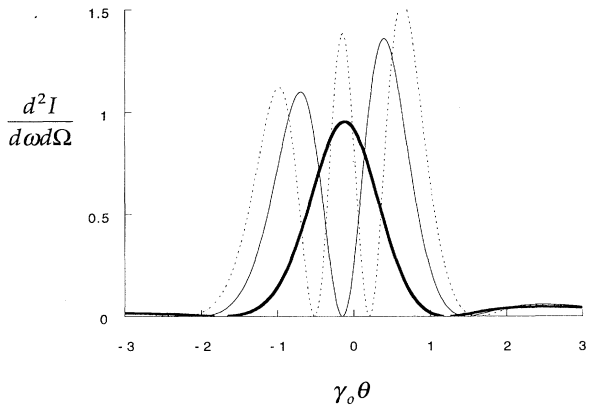

FIG. 10. Linear polarization, transverse scattering, $\beta_{1y}=0$. Normalized intensity of the first three harmonics of Fig. 9 along the x' axis of the detector. Distance along the axis is measured in units of $\gamma_0(x'/z_0')\sim\gamma_0\theta$.

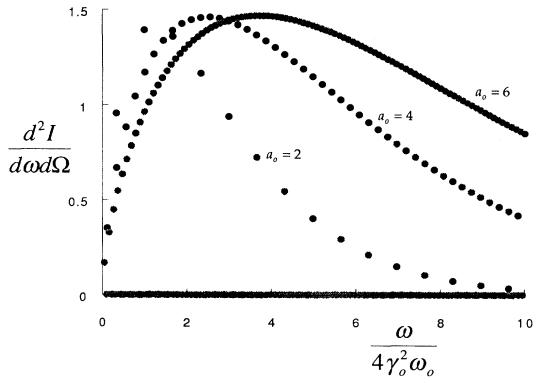

(a)

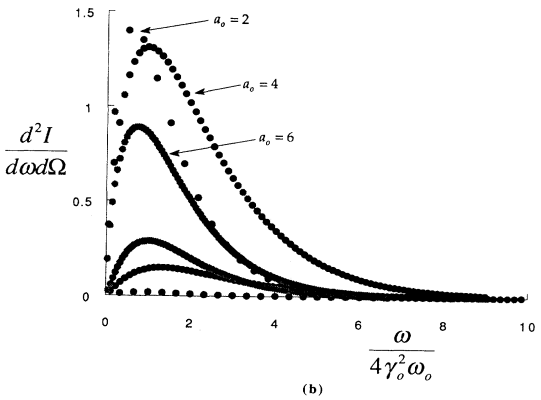

(b)

FIG. 11. (a) Intensity of odd harmonics on-axis ($\theta=0$) vs normalized frequency for a linearly polarized laser pulse, and head-on interaction. The results for $a_0=2$, 4, and 6 are shown. (b) Intensity of harmonics on-axis vs normalized frequency for a linearly polarized laser pulse, and transverse scattering, electron traveling in the y-z plane.

Again, a given harmonic appears at half the frequency of the corresponding harmonic in Fig. 11(a). The even harmonics do not vanish on-axis (although the intensity of an even harmonic on-axis is much below that of its off-axis peaks, which are not shown); note that the on-axis intensity in the even harmonics increases relative to that in the odd harmonics as a_0 is increased. In the case of transverse scattering when the electron is traveling in the plane of polarization, the central peaks of the harmonics do not fall on-axis (the radiation pattern is shifted slightly in x', see Fig. 10); thus the on-axis points fall under the envelope of the intensities of the central peaks.

VI. TOTAL SCATTERED FLUX AND PULSE LENGTH

The power radiated by a single electron undergoing relativistic quiver motion in an intense laser field can be calculated from the relativistic Larmor formula [36]

$$P=\frac{2e^2}{3c}\gamma^2\left[\left[\frac{d\mathbf{u}}{dt}\right]^2-\left[\frac{d\gamma}{dt}\right]^2\right] . \tag{42}$$

Assuming the electron orbit is a function of only the variable $\eta=z+ct$ and using the constant of motion $d(\gamma-u_z)/d\eta=0$ implies

$$P\approx\tfrac{1}{3}e^2ck_0^2a_0^2\gamma_0^2(1+\beta_{z0})^2 , \tag{43}$$

where an averaging over a laser period has been performed. The photon flux per electron (photons per second per electron) is found by dividing Eq. (43) by the average energy of the radiated photons: Flux$=P/\hbar\langle\omega\rangle$, where

$$\hbar\langle\omega\rangle=\frac{2(1+\beta_{z0})\gamma_0^2}{(1+a_0^2/2)}\langle n\rangle\hbar\omega_0 . \tag{44}$$

Here $\langle n\rangle$ is the average harmonic number and $\gamma_0^2\gg1$ has been assumed. The total number of photons radiated by a single electron N is found by multiplying the photon flux by the interaction time T. The single electron-laser interaction time can be expressed in terms of N_0, the number of laser periods with which the laser interacts, $cT=\lambda_0N_0/(1+\bar{\beta}_z)$. Hence, the number of radiated photons per electron is given by

$$N=\frac{\pi}{3}\alpha N_0a_0^2\frac{(1+a_0^2/2)(1+\beta_{0z})}{\langle n\rangle(1+\bar{\beta}_z)} , \tag{45}$$

where $\alpha=e^2/\hbar c=\frac{1}{137}$ is the fine structure constant. In the limit $a_0^2\ll1$, this reduces to

$$N\approx\alpha N_0a_0^2 . \tag{46}$$

The total number of photons generated, N_γ, is found by multiplying N by the total number of electrons, N_e, involved in the laser-electron beam interaction, i.e.,

$$N_\gamma \approx \alpha N_e N_0 a_0^2 \ . \tag{47}$$

The specific values for the total number of electrons radiating, and the total number of laser periods with which a single electron interacts with the laser field, depend on the particular geometry of the interaction.

Notice that the angular density of photons radiated from a single electron in the backscattered ($\theta=0$) direction, in the limits $a_0^2 \ll 1$ and $\gamma_0^2 \gg 1$, may be written as

$$\frac{dN}{d\Omega} \approx \alpha N_0 a_0^2 \frac{\gamma_0^2}{2}[1+(\cos\theta_I+\beta_{1x}\sin\theta_I)^2] \ . \tag{48}$$

This expression was derived using Eq. (27) and $N=I_1/\hbar\omega$. For either head-on ($\theta_I=0$) or transverse ($\theta_I=\pi/2$) scattering geometries, the quantity in the square brackets is ≈ 2. The half-angle of the radiation cone θ_C into which scattered photons are radiated, can be defined by $N \approx 2\pi\theta_C^2 dN/d\Omega$, where $dN/d\Omega$ is given by Eq. (48). Hence,

$$\theta_C \approx 1/(\gamma_0\sqrt{2\pi}) \ . \tag{49}$$

In the remainder of this section, the total number of photons generated, N_γ, as given by Eq. (47), and the duration of the scattered pulse τ_γ, will be estimated for two interaction geometries: head-on ($\theta_I=0$) and transverse ($\theta_I=\pi/2$). In the following, we consider a laser pulse with an axial (along the z axis) length L_0 and a transverse radius r_0, and include the effects of vacuum diffraction. For a laser pulse with a Gaussian radial profile of the form $\exp(-r^2/r_s^2)$, the spot size r_s of the field will evolve according to $r_s=r_0(1+z^2/Z_R^2)^{1/2}$, where $Z_R=\pi r_0^2/\lambda_0$ is the Rayleigh length and r_0 is the minimum spot size (radius) at the focal point $z=0$. Hence, Z_R is the characteristic distance over which a laser pulse with a focused spot size of r_0 will diffract. In the following, diffraction is assumed to limit the laser propagation to a distance of $2Z_R$. The electron beam is highly relativistic ($\gamma_0 \gg 1$), with a length L_b (along the z' axis) and a radius r_b (along the x' or y' axis). We assume that the electron beam and laser pulse are properly synchronized and aligned so as to optimize the interaction.

As noted previously, the total number of laser periods with which a single electron interacts is given by $N_0=(1+\bar{\beta}_z)cT/\lambda_0$, where $\bar{\beta}_z$ is the average axial electron velocity given by Eq. (12d). The time that a single electron interacts with the laser field T can be limited by (1) the axial pulse length of the laser, L_0, i.e., $cT=L_0/(1+\bar{\beta}_z)$, (2) the transverse dimension of the laser pulse $2r_0$, i.e., $cT=2r_0/\beta_{1\perp}$, or (3) the diffraction length of the laser pulse $2Z_R$, i.e., $cT=2Z_R/\bar{\beta}_z$. In general, the interaction time will be given by the minimum of these quantities, i.e.,

$$cT \approx \min[L_0/(1+\bar{\beta}_z), 2r_0/\beta_{1\perp}, 2Z_R/\bar{\beta}_z] \ . \tag{50}$$

The duration of the scattered radiation pulse will depend on the particular geometry of the interaction. Consider head-on interactions. For sufficiently short electron beams, $L_b < L_0, Z_R$, the scattered pulse duration is given by $c\tau_\gamma = L_b$, since the scattered radiation pulse and electron beam move essentially together. For long electron beams, the x-ray pulse duration will be limited by the spatial extent of the laser pulse, i.e., $c\tau_\gamma \approx 4Z_R + L_0$. Hence, for head-on interactions,

$$c\tau_\gamma \approx \min[L_b, (4Z_R + L_0)] \ . \tag{51}$$

For transverse interactions, $c\tau_\gamma = L_b$ for short electron beams ($L_b < L_0$), whereas $c\tau_\gamma \approx 2r_b + L_0$ or $2Z_R + L_0$ for long electron beams. Hence, for transverse interactions,

$$c\tau_\gamma \approx \min[L_b, 2r_b + L_0, 2Z_R + L_0] \ . \tag{52}$$

Similar arguments can be made to estimate the total number of electrons which interact with the laser field. Again, this depends on the specifics of the interaction geometry. It is convenient to express the total number of electrons involved in the interaction as $N_e=(I_b/e)f\tau_\gamma$, where I_b is the total electron beam current and f is a geometric filling factor (to properly account for the overlap between the electron beam and laser pulse); so $(I_b/e)f$ is the electron flux (electrons/second) in the direction of electron beam propagation. For head-on interactions, the filling factor is given by

$$f = \min[1, r_0^2/r_b^2] \ . \tag{53}$$

For transverse interactions, $f = f_{x'} f_{y'}$, where $f_{x'}$ and $f_{y'}$ are the filling factors in the x' and y' directions, respectively. Geometric arguments imply

$$f_{x'} \approx \min[1, L_0/2r_b, Z_R/r_b] \ , \tag{54a}$$

$$f_{y'} \approx \min[1, r_0/r_b] \ . \tag{54b}$$

As an example, consider x rays generated from head-on and transverse interactions between an electron beam and (i) a short-pulse (150 fs, $L_0=45$ μm) and (ii) a long-pulse (10 ps, $L_0=3$ mm) laser. An electron beam will be assumed with $\gamma_0=79$ (40 MeV), $L_b=1.5$ mm (5 ps), $r_b=50$ μm, and $I_b=200$ A. This corresponds to a total charge of 1 nC and a total electron flux of $I_b/e \approx 1.25\times10^{21}$ s^{-1}. The laser pulse parameters are $\lambda_0=1$ μm, $r_0=50$ μm, and a laser power of $P=10$ TW. This corresponds to $a_0=0.43$ and $Z_R=7.9$ mm. These parameters are summarized in Table I.

The wavelength of the backscattered x rays is $\lambda=\lambda_0/4\gamma_0^2 \approx 0.4$ Å (31-keV photons) for the head-on interaction, and $\lambda=\lambda_0/2\gamma_0^2 \approx 0.8$ Å (16-keV photons) for the transverse interaction. In both cases, the total x-ray flux will be confined to a cone of half-angle $\theta_C \approx 1/(\gamma_0\sqrt{2\pi}) \approx 5$ mrad. Using the above notation, the total number of scattered photons is given by

$$N_\gamma = \alpha(I_b/e)f\tau_\gamma N_0 a_0^2 \ . \tag{55}$$

Consider the short (150 fs) laser pulse example. For the head-on interaction, the total number of periods for which a single electron interacts with the laser is $N_0 \approx L_0/\lambda_0 = 45$, the filling factor is $f \approx 1$, and the x-ray pulse duration is $\tau_\gamma \approx L_b/c = 5$ ps. This implies a total x-ray flux of $N_\gamma = 3.8\times10^8$ photons. For the transverse interaction, $N_0 \approx L_0/\lambda_0 = 45$, $f_{x'} \approx L_b/2r_b = 0.45$, $f_{y'} \approx 1$, and $\tau_\gamma \approx (2r_b + L_0)/c = 480$ fs. This implies

TABLE I. Electron beam and laser parameters.

Electron beam parameters	
Beam energy E_b	40 MeV ($\gamma_0=79$)
Beam current I_b	200 A
Beam pulse length L_b/c	5 ps
Beam radius r_b	50 μm
Total charge Q_b	1 nC
Laser pulse parameters	
Wavelength λ_0	1 μm
Peak power P_0	10 TW
Spot size r_0	50 μm
Rayleigh length Z_R	7.9 mm
Intensity I_0	2.6×10^{17} W/cm^2
Strength parameter a_0	0.43
L_0/c, short-pulse case	150 fs
L_0/c, long-pulse case	10 ps

$N_\gamma=1.6\times10^7$ photons. These parameters are summarized in Table II.

Consider the long (10 ps) laser pulse example. For the head-on interaction, the total number of periods for which a single electron interacts with the laser is $N_0\approx L_0/\lambda_0=3000$, the filling factor is $f\approx1$, and the x-ray pulse duration is $\tau_\gamma\approx L_b/c=5$ ps. This implies a total x-ray flux of $N_\gamma=2.5\times10^{10}$ photons. For the transverse interaction, $N_0\approx2r_0/\lambda_0=100$, $f_{x'}\approx1$, $f_{y'}\approx1$, and $\tau_\gamma\approx L_b/c=5$ ps. This implies $N_\gamma=8.4\times10^8$ photons. These parameters are summarized in Table III.

VII. DISCUSSION

This paper presents a detailed theoretical description of nonlinear Thomson scattering of intense laser fields from relativistic electrons, extending previous colinear results to arbitrary interaction angles, with particular emphasis on the important case of transverse scattering. The theory is valid for linearly or circularly polarized incident laser fields of arbitrary intensities. Expressions for the intensity distributions of scattered radiation were calculated analytically; the intensity distributions were evaluated numerically for both head-on and transverse interaction geometries. Properties of the scattered radiation were examined, with particular attention given to the effect of interaction angle on the frequency and spatial distribution of the radiation. The effect of scattering angle on the radiated x-ray flux and pulse length was explored in some detail.

The intensity distributions derived in Sec. IV describe

TABLE II. X-ray parameters for the short-pulse laser.

X-ray pulse parameter	Head-on ($\theta_I=0$)	Transverse ($\theta_I=\pi/2$)
Photon wavelength λ	0.4 Å (30 keV)	0.8 Å (15 keV)
Filling factor f	$f=1$	$f_{x'}=0.45$, $f_{y'}=1$
Laser periods N_0	45	45
Photon pulse length τ_γ	5 ps	480 fs
Total photons N_γ	3.8×10^8	1.6×10^7

TABLE III. X-ray parameters for the long-pulse laser.

X-ray pulse parameter	Head-on ($\theta_I=0$)	Transverse ($\theta_I=\pi/2$)
Photon wavelength λ	0.4 Å (30 keV)	0.8 Å (15 keV)
Filling factor f	$f=1$	$f_{x'}=1$, $f_{y'}=1$
Laser periods N_0	3000	100
Photon pulse length τ_γ	5 ps	5 ps
Total photons N_γ	2.5×10^{10}	8.4×10^8

radiation emitted by a relativistic electron as a result of its nonlinear interaction with a high intensity laser pulse. In all cases, the radiation is emitted into a narrow cone about the electron's forward direction; the linewidth is narrow, depending (in the case of a single electron and neglecting variations in the laser intensity profile) on the number of laser periods the electron sees during the interaction. For the special case of head-on interactions, the results are familiar: if the light is circularly polarized, the fundamental peaks on-axis, all higher harmonics peak off-axis, vanish on-axis, and their intensity distributions are independent of ϕ; if the light is linearly polarized, the fundamental and all odd harmonics exhibit a peak on-axis, even harmonics vanish on-axis, and the radiation pattern of the nth harmonic has n peaks. For both types of polarization, the harmonics become important when $a_0\sim1$; if $a_0\gg1$, harmonics dominate the spectrum. If the electron and the laser pulse interact at an angle, both the frequency and spatial distribution of the scattered radiation are altered. The frequency of radiation into the nth harmonic, for both circular and linear polarization, is given by Eq. (38). The resonant frequency depends on the initial scattering angle as well as on the observation angle. This is familiar from inverse Compton scattering (in the low a_0 limit), and shows that the peak frequency of each harmonic decreases as the scattering angle increases. For transverse geometries, the frequency of backscattered radiation is a factor of 2 lower than it would be for head-on geometries.

For off-axis scattering, if the light is circularly polarized, a small amount of radiation appears on-axis in the higher harmonics; there is asymmetry in ϕ, which is most apparent in the higher harmonics. These effects increase with both angle and laser intensity. If the light is linearly polarized, and the electron is initially traveling in the y-z plane (perpendicular to the plane of polarization), then the spatial pattern is very similar to the colinear case. If the electron is initially traveling in the x-z plane, the entire pattern is shifted slightly in x', and the n peaks in the nth harmonic are now no longer symmetric about x'. These effects increase with both interaction angle and laser intensity.

A laser synchrotron source based on nonlinear Thomson scattering of intense lasers from relativistic electron beams may provide a means to produce tunable, narrow band x-ray radiation for use in a variety of practical and experimental applications. This type of source has several attractive features. It can be quite compact, because the electron beam need not be highly energetic; it can be tuned in frequency through a factor of 2 by chang-

ing the interaction angle, or over a wider factor by changing electron energy or employing harmonic radiation; it has a very narrow bandwidth $\Delta\omega/\omega \approx 1/N_0$ (in practice, bandwidth is limited by electron beam emittance); and it is capable of producing x rays in extremely short pulses (< 1 ps).

An LSS could be based on a colinear (or nearly colinear) geometry or on a transverse geometry. There are advantages to both. The colinear geometry produces scattered radiation at the highest frequency: that is, it would generate the highest frequency for a given electron energy, or would require the most modest electron energies if x rays of a given frequency were desired. Head-on interaction also results in the highest photon flux for a given laser pulse and electron beam because it results in the longest interaction time. The transverse geometry, on the other hand, allows the production of extremely short x-ray pulses [9], which could have important application in biology or medicine; the x-ray intensity is lower (because of the shorter interaction time), and the x rays produced have a lower energy (for a given energy electron beam), but as the example summarized in Table II illustrates, a 150-fs laser pulse and a 5-ps electron beam could produce an x-ray pulse of ~ 480 fs in duration.

In this paper we have calculated the radiation produced by a single electron as a result of its interaction with a square pulse of high intensity laser light. The intensity distribution resulting from the interaction of a real electron beam with a real laser pulse will be somewhat different as a result of the electron beam emittance and energy spread, and the shape of the laser pulse. For example, if the beam emittance is too large, the angular structure of the harmonic intensity distributions can be smeared out. The normalized emittance is given approximately by $\varepsilon_n = \gamma_0 r_b \theta_{\rm rms}$, where $\theta_{\rm rms}$ is the rms angular spread of the beam electrons. In order for the intensity peaks in the harmonic radiation to remain well defined, it is necessary that $\theta_{\rm rms} \ll \theta_{\rm peak}$, where $\theta_{\rm peak}$ is the angular separation between peaks. For the third harmonic (linearly polarized case), Figs. 6–10 indicate that $\theta_{\rm peak} \approx 1/\gamma_0$. Hence, resolution of the third harmonic intensity peaks requires $\varepsilon_n \ll 100$ mm mrad, assuming $r_b \approx 100$ μm. The effects of beam emittance and energy spread on the x-ray bandwidth and brightness have been discussed previously for the colinear case [1]; this paper provides the tools necessary to obtain detailed radiation patterns produced by lasers scattering off realistic electron beams. A detailed analysis of beam and laser pulse effects will be the subject of future work.

The results of this paper are directly relevant to several experiments (being planned or currently underway), which will explore Thomson scattering as a means of producing high frequency radiation [4,9,10,38–42]. Two of these experiments, one at the Institute of Laser Technology in Osaka [10] and the other at the Lawrence Berkeley Lab (LBL) [9,40], will employ off-axis scattering geometries. In Osaka, x rays will be produced by scattering the radiation stored in a Fabry-Pérot "super" cavity pumped by a high power, mode-locked Nd:YAG (yttrium aluminum garnet) laser; since the cavity is tilted with respect to the electron beam, the electrons and radiation will intersect at an angle. At LBL, researchers plan to scatter an ultrahigh power, subpicosecond laser pulse off a 50-MeV electron beam at right angles; this transverse geometry is being employed in order to generate subpicosecond x-ray pulses. The work presented here should be useful in interpreting the results of these experiments.

In addition, early results are available from experiments at the Naval Research Lab (NRL), where soft x rays (20 eV) have been produced by scattering high intensity laser pulses from a mildly relativistic (650 keV) electron beam [41]; this experiment is currently being upgraded to perform scattering off a higher energy (5 MeV) beam. Both the LBL and NRL experiments are using ultrahigh power, chirped-pulse amplification laser systems, which are capable of delivering laser pulses with $a_0 \geq 1$. Experiments using these ultrahigh laser intensities should provide experimental observation of nonlinear Thomson scattering.

ACKNOWLEDGMENTS

The authors would like to acknowledge useful discussions with P. Sprangle, A. Ting, W. Leemans, C. M. Tang, and G. Mourou. This work was supported by the Office of Naval Research and the Medical Free Electron Laser Program.

[1] E. Esarey, S. K. Ride, and P. Sprangle, Phys. Rev. E **48**, 3003 (1993).
[2] E. S. Sarachik and G. T. Schappert, Phys. Rev. D **1**, 2738 (1970).
[3] P. Sprangle, B. Hafizi, and F. Mako, Appl. Phys. Lett. **55**, 2559 (1989).
[4] F. Carroll, J. Waters, R. Price, C. Brau, C. Roos, N. Tolk, D. Pickens, and H. Stephens, Invest. Radiol. **25**, 465 (1990).
[5] P. Sprangle and E. Esarey, Phys. Fluids B **4**, 2241 (1992).
[6] P. Sprangle, A. Ting, E. Esarey, and A. Fisher, NRL, Report No. 6973, 1992 (unpublished); Stanford Synchrotron Radiation Laboratory, Report No. SSRL 92/02, 1992, p. 280 (unpublished); J. Appl. Phys. **72**, 5032 (1992).
[7] E. Esarey, P. Sprangle, A. Ting, and S. K. Ride, Nucl. Instrum. Methods Res. Sect. A **331**, 545 (1993).
[8] C.-M. Tang, B. Hafizi, and S. K. Ride, Nucl. Instrum. Methods Res. Sect. A **331**, 371 (1993).
[9] K. J. Kim, S. Chattopadhyay, and C. V. Shank, Nucl. Instrum. Methods Res. Sect. A **341**, 351 (1994).
[10] J. Chen, K. Imasaki, M. Fujita, C. Yamanaka, M. Asakawa, S. Nakai, and T. Asakuma, Nucl. Instrum. Methods Res. Sect. A **341**, 346 (1994); K. Imasaki *et al.*, *ibid.* **331**, 232 (1993).
[11] D. Strickland and G. Mourou, Opt. Commun. **56**, 216 (1985); P. Maine, D. Strickland, P. Bado, M. Pessot, and G. Mourou, IEEE J. Quantum Electron. **QE-24**, 398 (1988); F. Salin, J. Squier, and G. Vaillancourt, Opt. Lett. **16**, 1964 (1992).
[12] M. D. Perry, F. G. Patterson, and J. Weston, Opt. Lett.

15, 1400 (1990); F. G. Patterson and M. Perry, J. Opt. Soc. Am. B **8**, 2384 (1991).
[13] G. Mourou and D. Umstadter, Phys. Fluids B **4**, 2315 (1992); M. D. Perry and G. Mourou, Science **264**, 917 (1994).
[14] F. R. Arutyunian and V. A. Tumanian, Phys. Lett. **4**, 176 (1963).
[15] R. H. Milburn, Phys. Rev. Lett. **10**, 75 (1963).
[16] G. Fiocco and E. Thompson, Phys. Rev. Lett. **10**, 89 (1963).
[17] S. C. Chen and T. C. Marshall, IEEE J. Quantum Electron. **QE-21**, 924 (1985); Phys. Rev. Lett. **52**, 425 (1984).
[18] O. F. Kulikov *et al.*, Phys. Lett. **13**, 344 (1964).
[19] C. Bemporad *et al.*, Phys. Rev. **138**, B1546 (1965).
[20] C. K. Sinclair *et al.*, IEEE Trans. Nucl. Sci. **NS-16**, 1065 (1969).
[21] L. Federici *et al.*, Nuovo Cimento B **59**, 247 (1980).
[22] X. Yamazaki *et al.*, IEEE Trans. Nucl. Sci. **NS-32**, 3406 (1985).
[23] B. M. Kincaid, J. Appl. Phys. **48**, 2684 (1977).
[24] S. K. Ride and W. B. Colson, Stanford University High Energy Physics Laboratory, Report No. 858, 1979 (unpublished).
[25] W. B. Colson, IEEE J. Quantum Electron. **QE-17**, 1417 (1981).
[26] W. B. Colson, G. Dattoli, and F. Ciocci, Phys. Rev. A **31**, 828 (1985).
[27] D. F. Alferov, Y. A. Bashmakov, and E. G. Bessonov, Phys. Tech. Phys. **18**, 1336 (1974).
[28] P. Elleaume, *Laser Handbook: Free Electron Lasers,* edited by W. B. Colson, C. Pellegrini, and A. Renieri (Elsevier, Amsterdam, 1990), Vol. 6, Chap. 4.
[29] K. J. Kim, in *Physics of Particle Accelerators,* edited by M. Month and M. Dienes, AIP Conf. Proc. No. 184 (AIP, New York, 1989), Vol. I, p. 565.
[30] H. Winick, in *Physics of Particle Accelerators* (Ref. [29]), Vol. II, p. 2138.
[31] S. Krinsky, in *Proceedings of the 1991 IEEE Particle Accelerator Conference* edited by M. Allen (IEEE, New York, 1991), Vol. I, p. 11.
[32] A. Jackson, in *Proceedings of the 1991 IEEE Particle Accelerator Conference* (Ref. [31]), Vol. IV, p. 2637.
[33] P. Sprangle and E. Esarey, Phys. Rev. Lett. **67**, 2021 (1991); Phys. Rev. A **45**, 5872 (1992).
[34] P. Sprangle, E. Esarey, and A. Ting, Phys. Rev. Lett. **64**, 2011 (1990); Phys. Rev. A **41**, 4463 (1990); Phys. Fluids B **2**, 1390 (1990).
[35] L. D. Landau and E. M. Lifshitz, *The Classical Theory of Fields,* 3rd ed. (Pergamon, New York, 1971).
[36] J. D. Jackson, *Classical Electrodynamics,* 2nd ed. (Wiley, New York, 1975), Chap. 14.
[37] G. N. Watson, *A Treatise on the Theory of Bessel Functions* (Cambridge University Press, Cambridge, England, 1966).
[38] C. A. Brau (private communication).
[39] J. M. J. Madey (private communication).
[40] W. Leemans (private communication).
[41] A. Ting, R. Fischer, A. Fisher, K. Evans, R. Burris, J. Krall, E. Esarey, and P. Sprangle, J. Appl. Phys. **78**, 575 (1995).
[42] D. D. Meyerhofer (private communication).

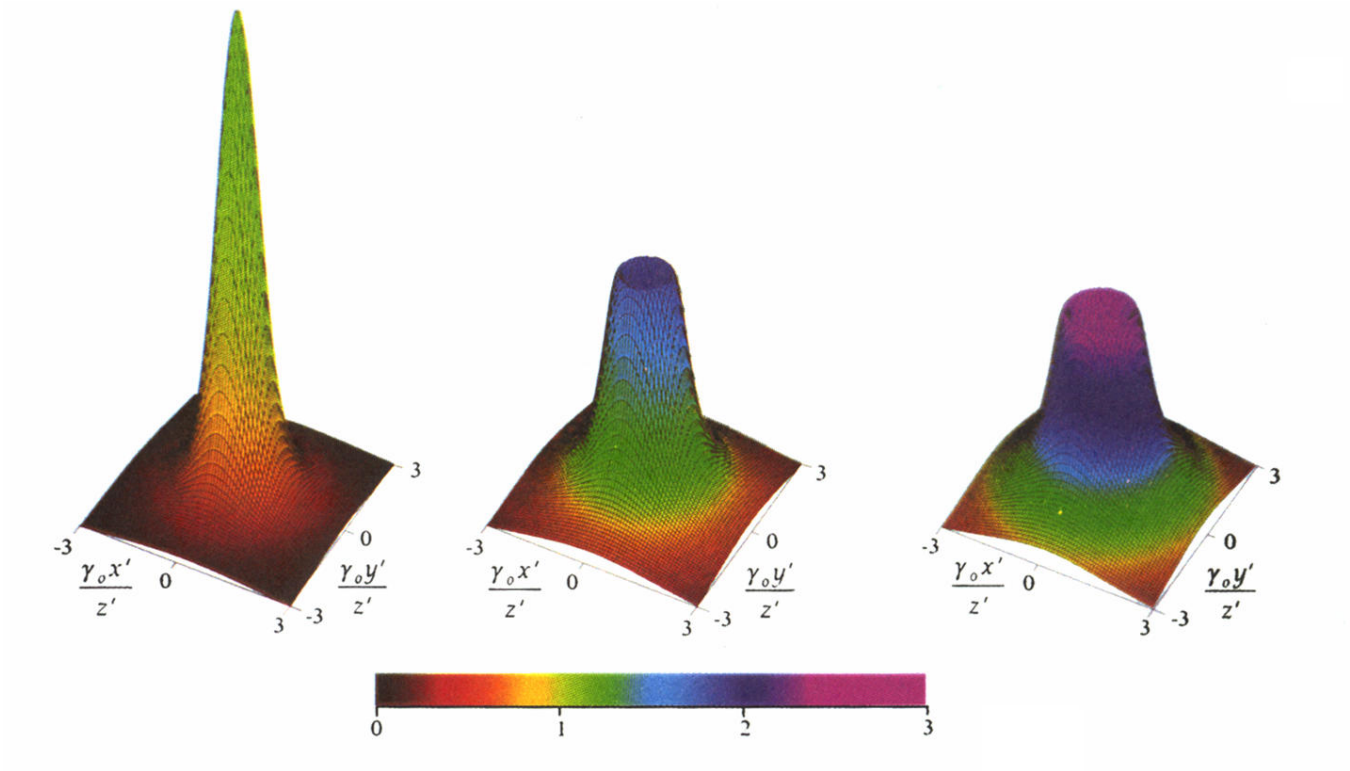

FIG. 3. Circular polarization, head-on scattering. The normalized intensity of radiation scattered by a relativistic electron ($\gamma_0=10$) from a counterpropagating ($\theta_I=0$) high intensity ($a_0=2$) circularly polarized laser pulse, viewed in the plane of a detector. The detector is located at z_0', and centered on the z' axis [backscattered radiation ($\theta=0$) falls on the center of the detector]. Distances in x',y' are measured in units $\gamma_0(x'/z_0')$, $\gamma_0(\gamma'/z_0')\sim\gamma_0\theta$. The three figures show the radiation into the first three harmonics (a) $n=1$; (b) $n=2$; (c) $n=3$. The color scale, marked in units of $4\gamma_0^2\omega_0/(1+a_0^2/2)$, indicates frequency of the scattered radiation.

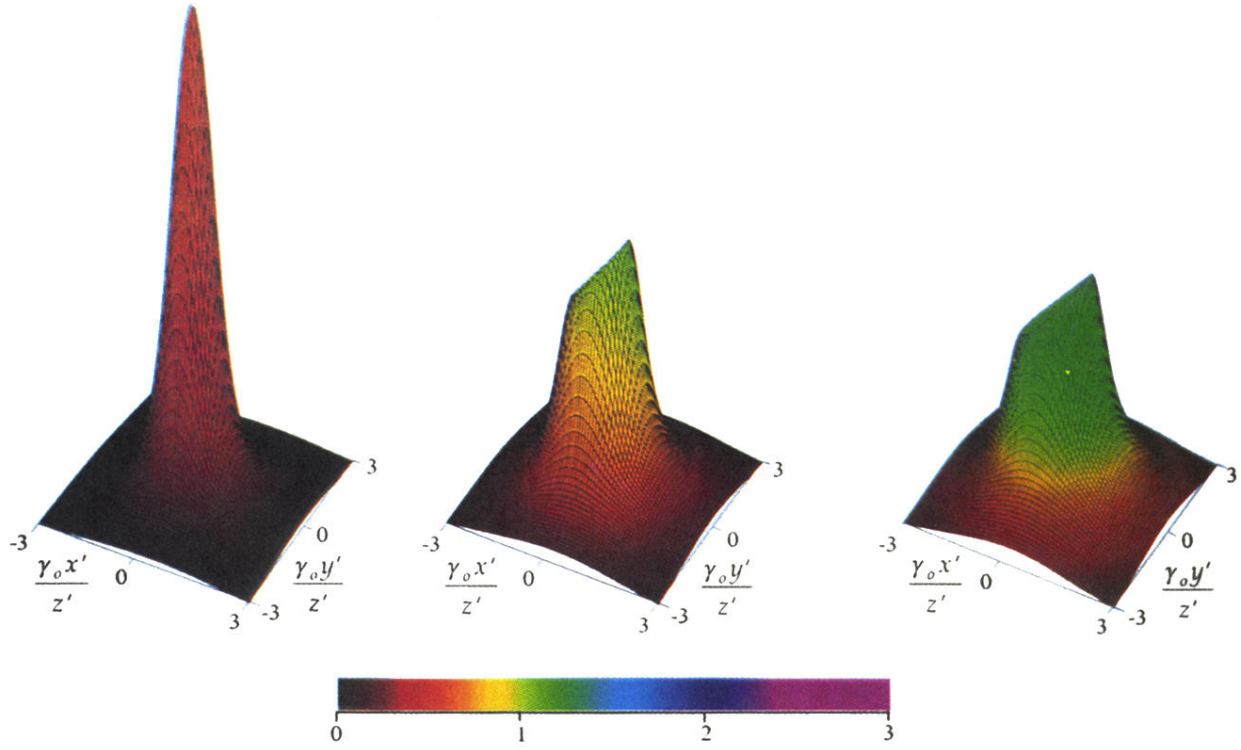

FIG. 4. Circular polarization, transverse scattering. The normalized intensity of radiation scattered by a relativistic electron ($\gamma_0=10$) from a transversely propagating ($\theta_I=90°$), high intensity ($a_0=2$) circularly polarized laser pulse, viewed in the plane of the detector. The detector is centered at z_0' along the z' ($\theta=0$) axis. Distances in x',y' are measured in units $\gamma_0(x'/z_0')$, $\gamma_0(y'/z_0')\sim\gamma_0\theta$. The three figures show radiation into the first three harmonics (a) $n=1$; (b) $n=2$; (c) $n=3$. The color scale, marked in units of $4\gamma_0^2\omega_0/(1+a_0^2/2)$, indicates frequency of the scattered radiation.

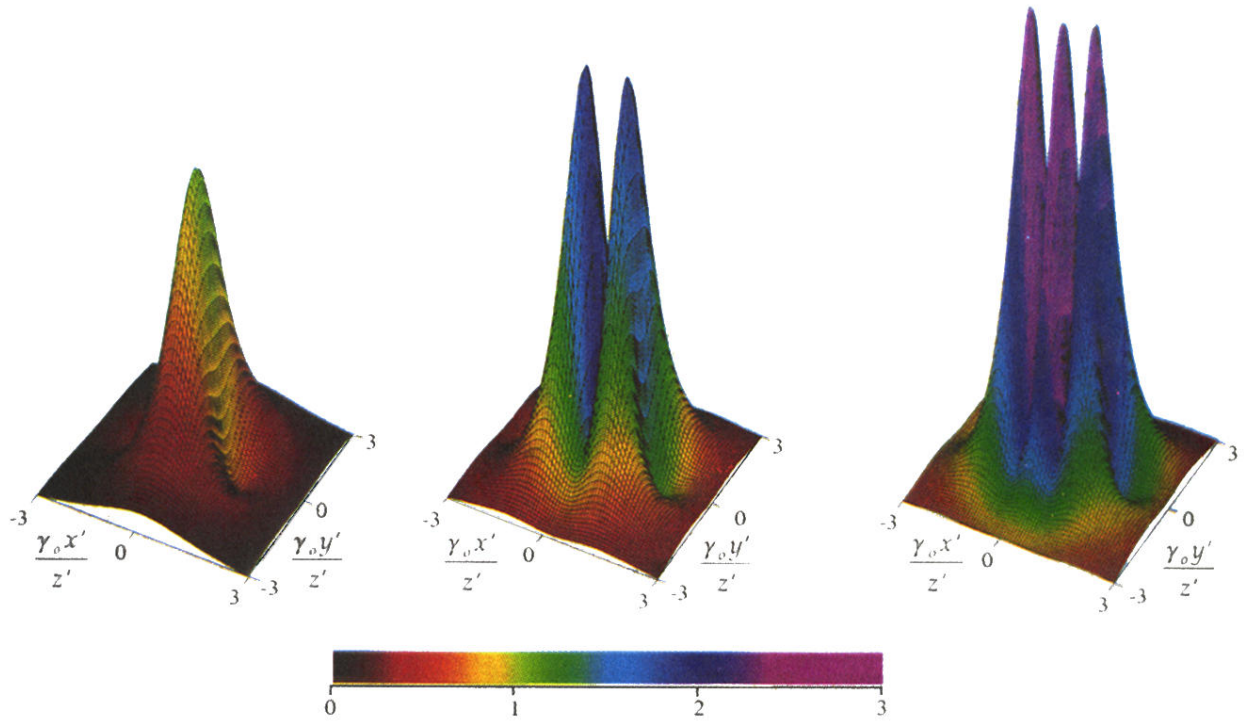

FIG. 6. Linear polarization, head-on scattering. The normalized intensity of radiation scattered by a relativistic electron ($\gamma_0=10$) from a counterpropagating $\theta_I=0$, high intensity ($a_0=2$) linearly polarized laser pulse, viewed in the plane of the detector. The detector is centered at z_0' along the z' ($\theta=0$) axis. Distances in x',y' are measured in units $\gamma_0(x'/z_0')$, $\gamma_0(y'/z_0')\sim\gamma_0\theta$. The three figures show radiation into the first three harmonics (a) $n=1$; (b) $n=2$; (c) $n=3$. The color scale, marked in units of $4\gamma_0^2\omega_0/(1+a_0^2/2)$, indicates frequency of the scattered radiation.

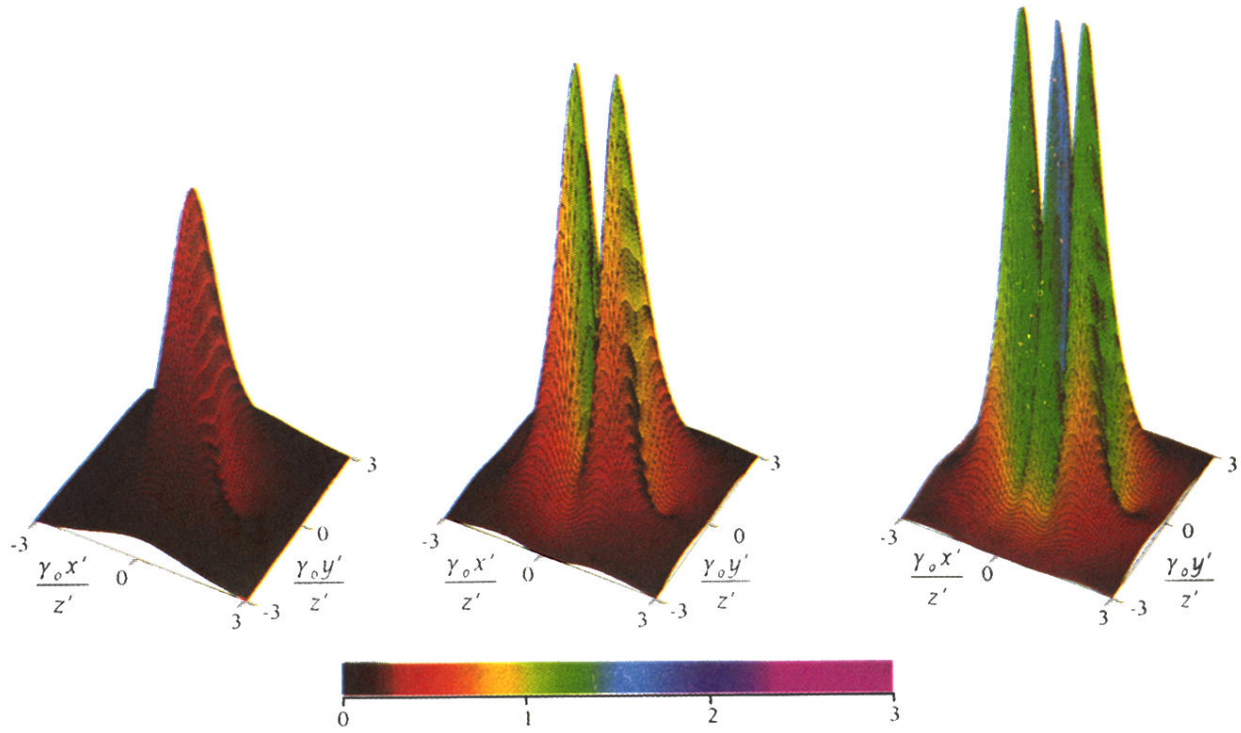

FIG. 7. Linear polarization, transverse scattering ($\beta_{1x}=0$). The normalized intensity of radiation into the first three harmonics emitted by a relativistic electron ($\gamma_0=10$) during interaction with a high intensity ($a_0=2$), linearly polarized laser pulse for an interaction angle of 90°. In this case, the electron is traveling perpendicular to the plane of laser polarization. The detector is centered at z_0' along the z' ($\theta=0$) axis. Distances in x',y' are measured in units $\gamma_0(x'/z_0')$, $\gamma_0(\gamma'/z_0')\sim\gamma_0\theta$. The color scale, marked in units of $4\gamma_0^2\omega_0/(1+a_0^2/2)$, indicates the frequency of the scattered radiation.

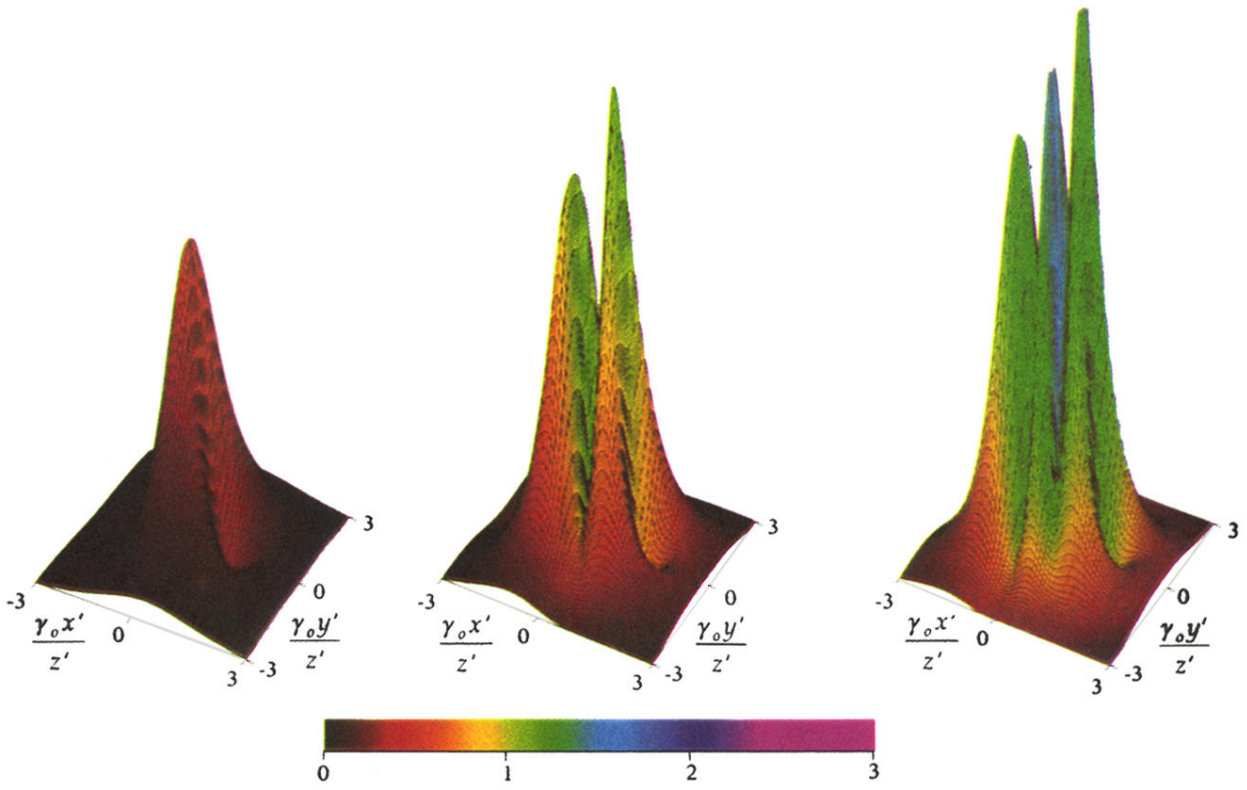

FIG. 9. Linear polarization, transverse scattering, $\beta_{1y}=0$. Same as in Fig. 7, but for the case of the electron traveling in the x-z plane (in the plane of polarization).